Outage Constrained Robust Beamforming Optimization for Multiuser IRS-Assisted Anti-Jamming Communications With Incomplete Information

Yifu Sun, Kang An, Junshan Luo, Yonggang Zhu, Gan Zheng, *Fellow, IEEE,* and Symeon Chatzinotas, *Senior Member, IEEE*

***Abstract*—Malicious jamming attacks have been regarded as a serious threat to Internet of Things (IoT) networks, which can significantly degrade the quality of service (QoS) of users. This paper utilizes an intelligent reflecting surface (IRS) to enhance anti-jamming performance due to its capability in reconfiguring the wireless propagation environment via dynamicly adjusting each IRS reflecting elements. To enhance the communication performance against jamming attacks, a robust beamforming optimization problem is formulated in a multiuser IRS-assisted anti-jamming communications scenario with or without imperfect jammer's channel state information (CSI). In addition, we further consider the fact that the jammer's transmit beamforming can not be known at BS. Specifically, with no knowledge of jammers transmit beamforming, the total transmit power minimization problems are formulated subject to the outage probability requirements of legitimate users with the jammer's statistical CSI, and signal-to-interference-plus-noise ratio (SINR) requirements of legitimate users without the jammer's CSI, respectively. By applying the Decomposition-based large deviation inequality (DBLDI), Bernstein-type inequality (BTI), Cauchy-Schwarz inequality, and penalty non-smooth optimization method, we efficiently solve the initial intractable and non-convex problems. Numerical simulations demonstrate that the proposed anti-jamming approaches achieve superior anti-jamming performance and lower power-consumption compared to the non-IRS scheme and reveal the impact of key parameters on the achievable system performance.**

***Index Terms*—Internet of Things (IoT), anti-jamming communications, intelligent reflecting surface (IRS), robust beamforming optimization, imperfect channel state information (CSI) .**

I. Introduction

INTERNET of Things (IoT) technology realizes massive connectivity for the unprecedented proliferation of devices, where a massive number of wireless devices are deployed to connect to a base station (BS) that is capable of sensing, communications and computations [1], [2]. However, due to the inherent propagation properties of wireless channels, IoT networks are increasingly vulnerable to jamming attacks [3]. In such attacks, a malicious third-party node injects jamming power into the legitimate users, hindering the legitimate transmissions by decreasing the signal-to-interference-plus-noise ratio (SINR) [4]. Thus, anti-jamming ability is an vital requirement for IoT networks.

In the past decades, various technologies have been developed to tackle the jamming attacks in IoT networks, such as channel hopping, power control, adaptive nulling antennas. Channel hopping is based on the concept that the cooperative communications parties switch their current working channel in a pseudorandom fashion to avoid the jamming signal's [5]–[12]. In [5], [8]–[10], game theory based channel hopping approaches were presented to obtain he optimal channel selection strategies, which model and analyze the interaction between users and jammers. For example, the authors in [5] proposed a defending strategy against jamming attacks in health monitoring IoT networks, where the orthogonal frequency-division multiplexing (OFDM) system and slow fading channels were considered. The authors in [11], [12] employed reinforcement learning (RL) to achieved the optimal channel hopping scheme without the knowledge of the jamming model. However, channel hopping does not optimally utilize the available spectrum and experiences the difficulty in reconstructing the communication links. Besides channel hopping, power control is another efficient anti-jamming approaches [13]–[16]. In [13]–[15], game-theoretic based optimal power control policies were obtained to combat the jamming attacks directly. An optimal transmit power scheme was provided in [16] to optimize the system rate by meeting the requirements of quality of service (QoS) for users. Netherless, owing to the limitation of user's energy supply, power control is only suitable for cases where the jamming power is limited. Moreover, adaptive nulling antennas technique can also be used to eliminate jamming signal, where the users employ a spatial filter to position the jamming signal is in the null space of the received signal [17], [18].

This work is supported by the National Natural Science Foundation of China under Grant U19B214 and 61901502, in part by the Foundation strengthening Plan Area Fund under Grant 2019-JCJQ-JJ-212 and Grant 2019-JCJQ-JJ226, in part by the National Postdoctoral Program for Innovative Talents under Grant BX20200101, partly funded by FNR RISOTTI, and in part by the Research Project of NUDT under Grants ZK18-02-11. *(Corresponding author: Yonggang Zhu; Kang An)*

Y. Sun, K. An, and Y. Zhu are with the Sixty-Third Research Institute, National University of Defense Technology, Nanjing 210007, China (Email: sunyifu.nudt@nudt.edu.cn; ankang89@nudt.edu.cn; zhumaka1982@163.com).

J. Luo is with the College of Electronic Science, National University of Defense Technology, Changsha 410005, China (Email: ljsnudt@foxmail.com).

G. Zheng is with the Wolfson School of Mechanical, Electrical and Manufacturing Engineering, Loughborough University, Loughborough LE11 3TU, U.K. (e-mail: g.zheng@lboro.ac.uk).

S. Chatzinotas is with Interdisciplinary Centre for Security, Reliability and Trust, University of Luxembourg, Luxembourg, L-1855, Luxembourg (e-mail: symeon.chatzinotas@uni.lu).

To address the abovementioned shortcomings, inteligent reflecting surface (IRS), which is also known as large intelligent surface (LIS) or reconfigurable intelligent surface (RIS), has been proposed as a promising technique to improve the anti-jamming performance in the IoT networks [19]. In particular, IRS is a reconfigurable metasurface consisting of many low-cost passive reflecting elements, where each element can independently reconfigure the propagation environment of the electromagnetic waves by imposing an phase shift and/or amplitude to the incident signal [20], [21]. As a result, IRS can enhance the the spectral and energy efficiency via jointly designing the active beamforming at the BS and passive beamforming at the IRS [22]–[25]. The works in [23] and [25] investigated the enhancement of IRS-assisted communications systems in fifth-generation (5G) communication. Specifically, aiming to improve the coverage and energy-efficiency of wireless network, the transmit beamforming and phase shift were jointly optimized to minimize the transmit power. In [26]–[29], the authors used IRS to maximize the secrecy rate in the presence of unauthorized eavesdroppers. In [30], aimming to maximize the weighted sum rate in the IRS-aided THz MIMO-OFDMA IoT networks, the authors proposed a robust beamforming and reflection matrix design scheme to optimize hybrid analog/digital beamforming. The authors in [31] first utilized the IRS to improve the anti-jamming performance of wireless communication, where the system achievable rate was maximized against jamming attacks. However, the aforementioned contribution [31] was based on the assumption that the perfect jammer's CSI and transmit beamforming are available to the transmitter. Unfortunately, due to the lack of cooperation between the legitimate users and jammers, it is challenging to obtain the perfect jammer's CSI and transmit beamforming [32]. To address this issue, in our previous work [33], we investigated an IRS-enhanced secure communication system for protecting the wireless transmission from both jamming and eavesdropping attacks, where the third-party nodes CSI is not perfectly known at the BS and the jammers transmit beamforming can not be obtained by the syetem. Nevertheless, [33] only considered the single-user case with bounded CSI error model, which is not applicable to the multi-user anti-jamming communications case with the statistical CSI model.

Currently, there are limited contributions related to the IRS-based wireless networks with imperfect CSI [34]–[39]. In [34] and [35], the authors investigated the robust beamforming design based on both the statistical CSI and the bounded CSI error models. In [38], under the imperfect CSI of the direct and cascaded channels, the authors investigated the robust beamforming design in a secrecy multiple-input single-output (MISO) network aided by the intelligent reflecting surface (IRS) with simultaneous wireless information and power transfer (SWIPT), where the minimum robust information rate among the legitimate information receivers (IRs) was maximized. In addition, under the assumption that the bounded CSI can be obtained by the access point (AP), the authors in [39] investigated robust and secure MISO downlink communications assisted by a self-sustainable intelligent reflection surface (IRS), which can simultaneously reflect and harvest energy from the received signals.

Motivated by these aforementioned observations, this paper investigates the robust beamforming at both BS and IRS in multiuser anti-jamming communications system. The main contributions of this paper are summarized as follows:

- A generalized model of robust optimization design in IRS-based multiuser anti-jamming system is proposed for the cases with statistical jammer's CSI or without jammer's CSI. In addition, we further consider the fact that the jammer's transmit beamforming can not be known at BS. Specifically, the active transmit beamforming at base station (BS) and the passive reflecting beamforming at IRS are jointly optimized to minimize total transmit power with incomplete information, while meeting the unit-modulus constraints, the requirement of each user's QoS requirements.
- For the case that jammer's statistical CSI is available, we aim to minimize the transmit power subject to the outage probability constraints and reflection phase constraints. Owing to the intractable optimization problem caused by the incompleted information, we first utilize the use-and-then-forget (Uatf) method and Cauchy-Schwarz inequality to address the issue that jammer's transmit beamforming are unknown at BS, and then use two inequalities to approximate the outage probability constraints so that the CSI uncertainty is tackled. Next, under the alternative optimization (AO) framework, the transmit beamforming and the reflecting beamforming are optimized iteratively by utilizing a penalty non-smooth optimization.
- For the case that jammer's CSI is unavailable, we formulate a robust beamforming optimization problem that minimizes the transmit power subjects to the SINR requirement and unit-modulus constraints. To achieve low computational complexity for practical implementation, we convert the transmit power minimization problem into the weighted channel gain maximization problem. Then, by applying AO, the high-quality beamforming is efficiently obtained through a penalty non-smooth optimization method.
- Numerical results demonstrate that, with the assistance of the IRS, the proposed approaches can achieve superior anti-jamming performance in terms of the minimum total transmit power and jamming margin[1] compared with the schemes without IRS. In addition, the number of IRS elements should be carefully chosen for achieving a satisfactory trade-off between the total transmit power and the feasibility probability of the formulated problem. Specifically, when the jammer's CSI estimation error is fixed, increasing the number of phase shifts can reduce the total transmit power, while a large number of IRS element will lead to a high infeasibility probability. Moreover, the high level of the CSI error will result in low system performance, and DBLDI-based approach outperforms the other two approaches in this scenario.

[1]Jamming margin denotes the maximum jamming power that the system can tolerate [40]. Specifically, minimizing transmit power means that we can use lower power to combat the same level of jamming power compared with Non-IRS scheme, and thus the jamming margin is improved when the user's energy supply is fixed.

Compared to the related work [39], the differences between our paper and [39] are three-fold. First, the two paper address different issues, which leads to different challenges in addressing the two problems. Specifically, [39] considered the system model that a BS transmits the independent data streams to multi-users in the presence of the potential eavesdroppers, while our paper considered that a BS with the assistance of an IRS wishes to reliably convey information to single-antenna multi-users in the presence of a malicious jammer. The different issues lead to different challenges, namely, the different security constraints and different assumptions. In particular, [39] considered the bounded CSI can be obtained by the BS, whereas our paper not only adopted the assumption that the jammers statistical CSI can be obtained but also considered the fact that the BS has no knowleage of jamming beamforming, which constitutes another unique challenge for address our considered issue. Second, the optimization objectives and the CSI error model of two paper are different, where [39] aimed to maximize the system achievable rate subject to the transmit power constraints, while our paper tries to minimize the total transmit power. Besides, the former assumed that the CSI error model is deterministic, namely the bounded CSI which characterizes the channel quantization error, while our paper assumed that the CSI error follows a circularly symmetric complex Gaussian distribution, i.e., the statistical CSI. Third, the solutions adopted in two paper are different. [39] first adopted the S-Procedure to address the CSI uncertainty, and then the successive convex approximation (SCA) with semi-definite relaxation (SDR) was proposed to the formulated problem with the rank-one constraint. However, our paper first utilize Uatf method and Cauchy-Schwarz inequality to address the issue that jammers transmit beamforming which is unknown at BS, and then use two inequalities to approximate the outage probability constraints so that the CSI uncertainty is tackled. Next, under the AO framework, the transmit beamforming and the reflecting beamforming are optimized iteratively by utilizing a penalty non-smooth optimization.

The remainder of this work is organized as follows. In Section II, we introduce the system model and the channel model. Section III presents the robust beamforming design for anti-jamming communications with the jammer's statistical CSI. Section IV presents the robust beamforming design without the jammer's CSI. In Section V, we compare the computational complexities of the proposed methods. Numerical results are provided in Section VI, where the best deployment of the IRS's location is also examined. We conclude this paper in Section VII.

Notation: $\mathbf{X}^H$, $\mathbf{X}^T$, $\mathbf{X}^*$, and $\|\mathbf{X}\|_F$ denote conjugate transpose, transpose, conjugate, and Frobenius norm of a matrix $\mathbf{X}$. The notations $\mathrm{E}\{\cdot\}$, $\mathrm{Tr}\{\cdot\}$, $\mathrm{Re}\{\cdot\}$, and $\lambda\{\cdot\}$ denote the expectation, trace, real part, and eigenvalue of a complex number or matrix, respectively. $\mathbb{C}^{m\times n}$ represents the complex space of $m\times n$ dimensions. The symbol $\mathbb{H}^{n\times n}$ is the Hermitian matrix of $n\times n$ dimensions. $[\cdot]_{n,n}$ represents the nth diagonal element of a matrix. $\mathbf{X}\succeq 0$ means that the matrix $\mathbf{X}$ is positive semi-definite. $\mathbf{X}\otimes\mathbf{Y}$ denotes the Kronecker product between two matrices $\mathbf{X}$ and $\mathbf{Y}$. $\langle\mathbf{X},\mathbf{Y}\rangle$ represents $\mathrm{Tr}\{\mathbf{X}^H\mathbf{Y}\}$. The distribution of a circularly symmetric complex Gaussian (CSCG) random vector with mean vector x and covariance matrix Σ is denoted by $\mathcal{CN}(x,\Sigma)$.

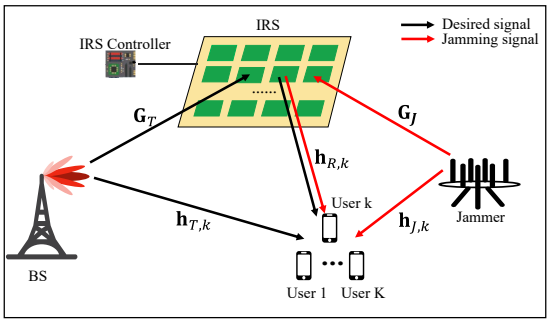

Fig. 1: System model of an IRS-assisted anti-jamming multiuser communications.

II. System Model

In this section, we first establish the system model of the IRS-assisted multiuser anti-jamming communications, and then introduce the channel model as well as the jammer's CSI uncertainty.

A. Signal Model

As shown in Fig. 1, this paper considers an IRS-assisted anti-jamming multiuser communication system, where a multi-antenna BS with the assistance of an IRS wishes to reliably convey information to K single-antenna users in the presence of a malicious multi-antenna jammer. It is assumed that the BS is equipped with M active antennas, and transmits the desired signal to all the users. An IRS with N passive reflecting elements is utilized to enhance the desired signal power and mitigate the jamming interference. Additionally, a jammer equipped with L antennas is located near the legitimate users degrading the QoS of users. For brevity, we define the users set as $\mathcal{K}=\{1,2,\cdots,K\}$ and the IRS reflecting elements set as $\mathcal{N}=\{1,2,\cdots,N\}$. The channel coefficients between the BS and the k-th user, between the BS and the IRS, between the IRS and the k-th user, between the jammer and the k-th user, and between the jammer and the IRS are denoted by $\mathbf{h}_{T,k}\in\mathbb{C}^{M\times 1}$, $\mathbf{G}_T\in\mathbb{C}^{N\times M}$, $\mathbf{h}_{R,k}\in\mathbb{C}^{N\times 1}$, $\mathbf{h}_{J,k}\in\mathbb{C}^{L\times 1}$, and $\mathbf{G}_J\in\mathbb{C}^{N\times L}$, respectively.

The transmitted signal at the BS intended for the k-th user is $s_{T,k}$ with unit average power $\mathrm{E}\left\{|s_{T,k}|^2\right\}=1$, which is weighted by the transmit beamforming vector $\mathbf{w}_{T,k}\in\mathbb{C}^{M\times 1}$. Thus, the overall transmitted signal $\mathbf{x}$ can be given by

$$\mathbf{x}=\sum_{k=1}^{K}\mathbf{w}_{T,k}s_{T,k}. \tag{1}$$

Let us assume that a multi-antenna jammer attempts to interrupt the communications by sending the jamming signal $\mathbf{w}_J s_J\in\mathbb{C}^{L\times 1}$ to the user's group, where $\mathrm{E}\left\{|s_{J,k}|^2\right\}=1$ and it cannot be obtained by the BS. Each IRS element receives the superimposed signal from the BS and the jammer, and reflects it to all the users. Let $\mathbf{\Phi}=$

$\text{diag}\left(A_1 e^{j\theta_1}, A_2 e^{j\theta_2}, \cdots, A_N e^{j\theta_N}\right)$ denote the reflection coefficient matrix, where $\theta_n \in [0, 2\pi)$ and $A_n \in [0, 1]$ denote the phase shift and the amplitude reflection coefficient of the nth element of the IRS, respectively. Here, we set $A_n = 1, \forall n$ as in [23], [33], [39], [41] for simplicity.[2][3] Due to the high path-loss, the signal which has been reflected by the IRS twice or more times can be ignored. It is assumed that the feedback channels between the BS and the IRS controller is dedicated [34], [44]. As such, for the k-th user, the received signal consists of the signal coming from the BS, the jamming signal from the jammer and the reflected superimposed signal from the IRS[4], which is given by (2) in at the top of the next page. In (2), the term $n_k \sim \mathcal{CN}(0, \sigma_k^2)$ denotes the additive white Gaussian noise (AWGN) with a zero-mean and variance σ_k^2. For subsequent analysis, we further adopt the the cascaded channel in the works [34] and [35] to denote the channel from the BS and the jammer to user via the IRS, i.e. $\mathbf{H}_{T,k} = \text{diag}(\mathbf{h}_{R,k}^H)\mathbf{G}_T$, $\mathbf{H}_{J,k} = \text{diag}(\mathbf{h}_{R,k}^H)\mathbf{G}_J, \forall k \in \mathcal{K}$. Denote by $\mathbf{W}_T = \{\mathbf{w}_{T,1}, \mathbf{w}_{T,2}, \cdots, \mathbf{w}_{T,K}\}$ the precoder matrix at the BS, by $\mathbf{v} = \{\text{v}_1, \text{v}_2, \cdots, \text{v}_N\}^H = \{e^{j\theta_1}, e^{j\theta_2}, \cdots, e^{j\theta_N}\}^H$ the phase shift vector at the IRS. Then, we have the SINR at k-th user, which is expressed as

$$\text{SINR}_k\left(\mathbf{W}_T, \mathbf{v}\right) = \frac{\left|(\mathbf{h}_{T,k}^H + \mathbf{v}^H\mathbf{H}_{T,k})\mathbf{w}_{T,k}\right|^2}{\sum\limits_{m\in\mathcal{K}, m\neq k}\left|(\mathbf{h}_{T,k}^H + \mathbf{v}^H\mathbf{H}_{T,k})\mathbf{w}_{T,m}\right|^2 + J_k + \sigma^2}, \quad (3)$$

where the term $J_k = \left|(\mathbf{h}_{J,k}^H + \mathbf{v}^H\mathbf{H}_{J,k})\mathbf{w}_J\right|^2$ denotes the received jamming power at the k-th user.

B. Channel Model and CSI Assumption

In the subsection, considering the small-scale fading, we assume the Rician fading channel model for all the channels involved. For example, the cascaded channel coefficient of BS-IRS- k-th user link $\mathbf{H}_{T,k}$ is expressed as

$$\mathbf{H}_{T,k} = \sqrt{\frac{\beta_{HT,k}}{1+\beta_{HT,k}}}\mathbf{H}_{T,k}^{\text{LoS}} + \sqrt{\frac{1}{1+\beta_{HT,k}}}\mathbf{H}_{T,k}^{\text{NLoS}}, \quad (4)$$

where $\beta_{HT,k}$ denotes the Rician factor; $\mathbf{H}_{T,k}^{\text{LoS}}$ is the line-of-sight (LoS) component; and $\mathbf{H}_{T,k}^{\text{NLoS}}$ is the Rayleigh fading component. The cascaded channel link above is dominated by the LoS component, which remains unchanged for a relatively long time due to their stationary position [45]. To account for large-scale fading, the distance dependent path loss model is adopted, i.e.,

$$LP = L_0\left(\frac{d}{D_0}\right)^{-\iota}, \quad (5)$$

where L_0 is the path loss at the reference distance D_0; d is the individual link distance; and the ι denotes the path loss exponent.

In the IRS-assisted anti-jamming communication system, there are two type of channels: the legitimate channels (i.e. $\mathbf{h}_{T,k}$ and $\mathbf{H}_{T,k}$) and the jamming channels (i.e. $\mathbf{h}_{J,k}$ and $\mathbf{H}_{J,k}$). For the legitimate channels, we can estimate the CSI accurately through calculating the angles of arrival and departure, or sending the pilot [41]. However, due to the lack of cooperation between the BS and the jammer, the jammer's channels and transmit beamforming are more challenging to acquire. In the following, we first deal with the outage-constrained robust beamforming problem with the incomplete information. Then, we further consider the robust beamforming design without jammer's information.

III. Outage Constrained Robust Beamforming Design with Incomplete Information

In this section, we assume that the CSI of all legitimate channels involved is perfectly available, and the jammer's statistical CSI can be obtained due to the slow-varying property of channels [46]. Thus, the robust beamforming design is proposed under the statistical jammer's CSI model.

A. Problem Formulation

The objective of our robust design is to minimize the total transmit power by jointly optimizing the active beamforming at the BS and the passive beamforming at the IRS, while ensuring the outage probability of each user is below the threshold for all possible jammer's CSI error realizations. By defining $\rho_k \in (0, 1]$ and $\gamma_k > 0$ as the outage probability and SINR target for user k respectively, the total power minimization problem should be expressed as

$$\mathcal{F}: \quad \min_{\mathbf{W}_T, \mathbf{v}} \|\mathbf{W}_T\|_F^2 \quad (6a)$$

$$s.t. \quad \Pr_{\{\mathbf{H}_{J,k}, \mathbf{h}_{J,k}\}}\left\{\text{SINR}_k\left(\mathbf{W}_T, \mathbf{v}\right) \geq \gamma_k\right\} \geq 1 - \rho_k, \forall k \in \mathcal{K}, \quad (6b)$$

$$0 \leq \theta_n \leq 2\pi, \forall n = 1, 2, \ldots N, \quad (6c)$$

[2] Although there are many practical models showing that the phase and amplitude of IRS elements are dependent on each othe [42], [43], this paper still set the reflection coefficient $A_n = 1, \forall n$, as commonly adopted in the literature, e.g., [23], [33], [39], [41]. The reason account for adopting the model is two-fold. First, [43] has demonstrated the negative impact of the correlation between θ_n and A_n on the system performance, and thus in practice, each element of the IRS is usually designed to maximize the signal reflection [23], [33], [39], [41]. Second, by referring to [43], the amplitude reflection can be controlled as approximate constant by designing the parameters the unit cells of RIS for practical implement. Thus, it is reasonable to assume that $A_n = 1, \forall n$. The impact induced by the correlation between θ_n and A_n on the proposed model will be left for our future work.

[3] Theoretically, the reflection amplitude of each element can be adjusted for different purposes such as channel estimation, anti-jamming, and performance optimization. However, in practice, it is costly to implement independent control of the reflection amplitude and phase shift simultaneously, and thus each element is usually designed to maximize the signal reflection for simplicity [23], [33], [39], [41]. As for the implement of both the amplitude and the phase, e.g., by equipping the reflecting elements with locally tunable integrated circuits (ICs) that provide a continuously tunable complex impedance [42], the full characterization of this case requires a full journal paper to be conceived in our future research.

[4] This paper considers the reflecting channel from the jammer to IRS, while the works in [31] ignored the fact that the jamming signal can also be reflected by the IRS in practice.

$$y_{r,k}=\underbrace{(\mathbf{h}_{T,k}^H+\mathbf{h}_{R,k}^H\mathbf{\Phi}\mathbf{G}_T)\mathbf{w}_{T,k}s_{T,k}}_{\text{desired signal}}+\underbrace{\sum_{m\in\mathcal{K},m\neq k}(\mathbf{h}_{T,k}^H+\mathbf{h}_{R,k}^H\mathbf{\Phi}\mathbf{G}_T)\mathbf{w}_{T,m}s_{T,m}}_{\text{inter-user interference}}+\underbrace{(\mathbf{h}_{J,k}^H+\mathbf{h}_{R,k}^H\mathbf{\Phi}\mathbf{G}_J)\mathbf{w}_Js_J}_{\text{jamming signal}}+n_k. \tag{2}$$

where the jammer's statistical CSI[5] for k-th user follows CSSG distribution[6] , which can be represented as

$$\mathbf{H}_{J,k}=\widehat{\mathbf{H}}_{J,k}+\Delta\mathbf{H}_{J,k},\text{vec}\left(\Delta\mathbf{H}_{J,k}\right)\sim\mathcal{CN}(0,\mathbf{\Sigma}_{HJ,k}),\ \mathbf{\Sigma}_{HJ,k}\succeq 0, \tag{7}$$

$$\mathbf{h}_{J,k}=\widehat{\mathbf{h}}_{J,k}+\Delta\mathbf{h}_{J,k},\Delta\mathbf{h}_{J,k}\sim\mathcal{CN}(0,\mathbf{\Sigma}_{hJ,k}),\mathbf{\Sigma}_{hJ,k}\succeq 0, \tag{8}$$

where $\mathbf{\Sigma}_{HJ,k}\in\mathbb{C}^{NL\times NL}$ and $\mathbf{\Sigma}_{J,k}\in\mathbb{C}^{L\times L}$ are the error covariance matrices.

Obviously, the problem $\mathcal{F}$ cannot be solved directly due to the coupled variables $\mathbf{W}_T$ and $\mathbf{v}$ in the outage probability constraints (6b). Additionally, the probabilistic problem does not have simple closed-form expressions, and the jammer's transmit beamforming cannot be obtained by BS. To solve the problem $\mathcal{F}$, an AO algorithm is proposed by utilizing use-and-then-forget (Uatf) method, Cauchy-Schwarz inequality, DBLDI, BTI, and penalty non-smooth optimization method [32], [49], [50]. For the convenience of further derivations, we first present two useful lemmas of DBLDI and BTI.

Lemma 1: (*Decomposition-Based Large Deviation Inequality [49]*) Assume $\mathbf{e}\in{}^{n\times 1}\sim\mathcal{CN}(0,\mathbf{I}_n)$ be a standard complex Gaussian random vector, $\mathbf{Q}\in\mathbb{H}^{n\times n}$, $\mathbf{r}\in\mathbb{C}^{n\times 1}$, and $s\in\mathbb{R}$. Then, for any $\rho\in(0,1]$, we have the DBLDI-based approximation, i.e.,

$$\begin{aligned}&\Pr\left\{\mathbf{e}^H\mathbf{Q}\mathbf{e}+2\text{Re}\left\{\mathbf{r}^H\mathbf{e}\right\}+s\geq 0\right\}\geq 1-\rho\\ \Leftrightarrow&\text{Tr}\left\{\mathbf{Q}\right\}-2\sqrt{\ln\left(1/\rho\right)}\left(\frac{1}{\sqrt{2}}\left\|\mathbf{r}\right\|+\beta\|\mathbf{Q}\|_F\right)+s\geq 0\end{aligned}$$

$$\Leftrightarrow\begin{cases}\text{Tr}\left\{\mathbf{Q}\right\}-2\sqrt{\ln\left(1/\rho\right)}\left(x+y\right)+s\geq 0\\ \frac{1}{\sqrt{2}}\|\mathbf{r}\|_2\leq x\\ \beta\|\mathbf{Q}\|_F\leq y\\ \left(1-1/\left(2\beta^2\right)\right)\beta=\sqrt{\ln\left(1/\rho\right)},\end{cases} \tag{9}$$

where x and y are slack variables, and the term "A $\Leftrightarrow$ B" denotes A is equivalent to B.

Proof: Please refer to [49] for the proof of Lemma 1.

Lemma 2: (*Bernstein-type Inequality [51]*) Assume $\mathbf{e}\in\mathbb{C}^{n\times 1}\sim\mathcal{CN}(0,\mathbf{I}_n)$ be a standard complex Gaussian random vector. Given $\mathbf{Q}\in\mathbb{H}^{n\times n}$, $\mathbf{r}\in\mathbb{C}^{n\times 1}$, and $s\in\mathbb{R}$, for any $\rho\in(0,1]$, the BTI-based approximation method holds:

$$\begin{aligned}&\Pr\left\{\mathbf{e}^H\mathbf{Q}\mathbf{e}+2\text{Re}\left\{\mathbf{r}^H\mathbf{e}\right\}+s\geq 0\right\}\geq 1-\rho\\ \Leftrightarrow&\text{Tr}\left\{\mathbf{Q}\right\}-\sqrt{2\ln\left(1/\rho\right)}x+\ln\left(\rho\right)\lambda_{\max}^{+}\left(-\mathbf{Q}\right)+s\geq 0\\ \Leftrightarrow&\begin{cases}\text{Tr}\left\{\mathbf{Q}\right\}-\sqrt{2\ln\left(1/\rho\right)}x+\ln\left(\rho\right)y+s\geq 0\\ \sqrt{\|\mathbf{Q}\|_F^2+2\|\mathbf{r}\|_2^2}\leq x\\ y\mathbf{I}+\mathbf{Q}\succeq 0,y\geq 0,\end{cases}\end{aligned} \tag{10}$$

where x and y are slack variables, and $\lambda_{\max}^{+}\left(-\mathbf{Q}\right)=\max\left(\lambda_{\max}\left(-\mathbf{Q}\right),0\right)$.

Proof: Please refer to [51] for the proof of Lemma 2.

Note that it has been shown in [49] and [51] that these two Lemmas and approximations are equivalent, which suggests that the approximations are tight. In addition, since the approximation based on DBLDI only contains SOC constraints, it can be solved more efficiently than the BTI-based approximation. In particular, when the size of linear matrix inequality (LMI) constraints is large, it is more costly to use the BTI-based approximation method in terms of the computational complexity and feasibility rate [49].

In the following subsections, an AO algorithm is proposed to solve the optimal $\mathbf{W}_T$ and $\mathbf{v}$ in an iterative manner. Specifically, we first design the transmit beamforming at the BS, and then optimize the reflecting beamforming by using the two lemmas above.

B. Tractable Countermeasure for Transmit Beamforming Design

In this subsection, we aim to optimize the transmit beamforming $\mathbf{W}_T$ so that the total transmit power is minimized with given phase shift $\mathbf{v}$. Since the jamming power $J_k=\left|(\mathbf{h}_{J,k}^H+\mathbf{v}^H\mathbf{H}_{J,k})\mathbf{w}_J\right|^2$ in (3) involves no terms of $\mathbf{W}_T$, we can regard it as a fixed power. Thus, the probabilistic constraints (6b) will be transformed into a SINR constraints,

[5]Although many existing works with IRS have considered deterministic CSI error model, namely the bounded CSI model, it only characterizes the channel quantization error which naturally belongs to a bounded region [34]. In this regards, we adopt the statistical CSI model due to the fact that the practical illegitimate CSI generally follows the CSSG distribution. As for the angular model, it only suitable for the geometric model, while this paper considered the Rician fading channel model.

[6]The reason why the assumption that the RIS-related error covariances follow the CSCG distribution is adopted can be divided into three-fold. First, according to the Secition II-B in [47], when the inter-element spacing between RIS units are set as the half-wavelength, the RIS-related CSI error covariances are i.i.d. CSCG distributed in the continuous phase-shift case. Second, according to [32], the statistical CSI of jammer is mainly depend on the direction of user-jammer channel, the antenna number of the jammer, and the path loss determined by the transmission distance, and and all of which is fixed in long-term time and can be pre-obtained by the jammer via the rotational invariance techniques and the law of cosines [48]. Thus, it is reasonable to consider that the jammer's statistical CSI can be obtained by the BS. In addition, due to the location error and white noise, the statistical CSI follows CSCG distribution around the accurate CSI with fixed location [32]. Third, as the widely adopted reason in the existing works, e.g., [38], in the time division duplex (TDD) setting, noise and limited training will cause the uplink channel estimation error. The conventional MMSE method is generally adopted to estimate the cascaded channel, and thus the channel estimation generally follows the CSCG distribution.

and the problem $\mathcal{F}$ corresponding to $\mathbf{W}_T$ is rewritten as

$$\mathcal{Q}_1^W: \min_{\mathbf{W}_T} \|\mathbf{W}_T\|_F^2 \tag{11a}$$

$$s.t. \frac{\left|(\mathbf{h}_{T,k}^H + \mathbf{v}^H\mathbf{H}_{T,k})\mathbf{w}_{T,k}\right|^2}{\sum\limits_{m\in\mathcal{K},m\neq k}\left|(\mathbf{h}_{T,k}^H + \mathbf{v}^H\mathbf{H}_{T,k})\mathbf{w}_{T,m}\right|^2 + J_k + \sigma^2} \geq \gamma_k, \forall k \in \mathcal{K}. \tag{11b}$$

It is found that problem $\mathcal{Q}_1^W$ can be efficiently solved by applying semidefinite program (SDP) [52], or second-order cone program (SOCP) [53]. In addition, the optimal solution to problem $\mathcal{Q}_1^W$ is obtained when all the SINR constraints (11b) are met with equalities [23]. Thus, by using SDP approaches and introducing the new variables $\tilde{\mathbf{h}}_{T,k} = (\mathbf{h}_{T,k}^H + \mathbf{v}^H\mathbf{H}_{T,k})^H$ and $PJ_k = J_k + \sigma_k^2$, the initial non-convex problem $\mathcal{Q}_1^W$ can be converted into a SDP problem, namely

$$\mathcal{Q}_2^W: \min_{\mathbf{\Gamma}_T} \sum_{k=1}^K \mathrm{Tr}\{\mathbf{\Gamma}_{T,k}\} \tag{12a}$$

$$s.t.\ \mathrm{Tr}\left\{\tilde{\mathbf{h}}_{T,k}\tilde{\mathbf{h}}_{T,k}^H\left(\frac{1}{\gamma_k}\mathbf{\Gamma}_{T,k} - \sum_{\substack{m\in\mathcal{K},\\ m\neq k}}\mathbf{\Gamma}_{T,m}\right)\right\} - PJ_k \geq 0, \forall k \in \mathcal{K}, \tag{12b}$$

$$\mathbf{\Gamma}_{T,k} \succeq 0,\ \forall k \in \mathcal{K}, \tag{12c}$$

$$\mathrm{rank}\,(\mathbf{\Gamma}_{T,k}) = 1,\ \forall k \in \mathcal{K}, \tag{12d}$$

where $\mathbf{\Gamma}_T = \{\mathbf{\Gamma}_{T,1}, \mathbf{\Gamma}_{T,2}, \cdots, \mathbf{\Gamma}_{T,K}\}$ and $\mathbf{\Gamma}_{T,k}{=}\mathbf{w}_{T,k}\mathbf{w}_{T,k}^H$.

Note that problem $\mathcal{Q}_2^W$ is still intractable due to the rank-one constraints (12d). The semidefinite relaxation (SDR) and Gaussian randomization (GR) approaches are commonly used method to tackle the rank-one constraints. However, the SDR may result in a lower bound of transmit power, and the GR method needs to generate sufficiently large number of random vectors for constructing a feasible rank-one beaforming $\mathbf{w}_{T,k}$. Apparently, the SDR with GR leads to a suboptimal or even far from the optimal solution. Hence, this paper utilizes the penalty non-smooth optimization method to deal with the rank-one constraints (12d), which has better performance than the SDR with GR [50].

It is observed that there are two additional constraints (12c) and (12d) introduced by the definition $\mathbf{\Gamma}_{T,k}{=}\mathbf{w}_{T,k}\mathbf{w}_{T,k}^H$ in problem $\mathcal{Q}_2^W$. Based on $\mathbf{\Gamma}_{T,k} \succeq 0$, we obtain $\mathrm{Tr}\{\mathbf{\Gamma}_{T,k}\} \geq \lambda_{\max}(\mathbf{\Gamma}_{T,k})$. If it also holds $\mathrm{Tr}\{\mathbf{\Gamma}_{T,k}\} - \lambda_{\max}\{\mathbf{\Gamma}_{T,k}\} \leq 0$, we can prove that $\mathrm{Tr}\{\mathbf{\Gamma}_{T,k}\}{=}\lambda_{\max}\{\mathbf{\Gamma}_{T,k}\}$, which suggests that $\mathbf{\Gamma}_{T,k}$ only have one non-zero eigenvalue. Therefore, the rank-one constraints (12d) can be equivalently expressed as

$$\mathrm{rank}\,(\mathbf{\Gamma}_{T,k}) = 1 \Leftrightarrow \mathrm{Tr}\{\mathbf{\Gamma}_{T,k}\} - \lambda_{\max}\{\mathbf{\Gamma}_{T,k}\} \leq 0. \tag{13}$$

Clearly, the rank-one constraints (12d) can be guaranteed by (13) in all cases. However, due to the property that $\mathrm{Tr}\{\mathbf{\Gamma}_{T,k}\}{-}\lambda_{\max}\{\mathbf{\Gamma}_{T,k}\}$ is concave, (13) is still a non-convex constraints. In particular, the term $\lambda_{\max}\{\mathbf{\Gamma}_{t,k}\}$ in (13) is convex related with the Hermitian matrix.

To address the issue above, we adopt the exact penalty method. Specifically, we first introduce the weight coefficients $\boldsymbol{\mu}{=}\{\mu_1, \mu_2, \cdots, \mu_k\}$ to enlarge the size of the feasible solution set spanned by constraint (13). Then we add the new goal into the objective function (12a) based on the penalty method. Accoding to [50], problem $\mathcal{Q}_2^W$ is equivalently rewritten as

$$\mathcal{Q}_3^W: \min_{\mathbf{\Gamma}_T} \sum_{k=1}^K \left((\mu_k{+}1)\,\mathrm{Tr}\{\mathbf{\Gamma}_{T,k}\} - \mu_k\lambda_{\max}\{\mathbf{\Gamma}_{T,k}\}\right) \tag{14}$$
$$s.t.\ (12b), (12c),$$

where $\mu_k > 0, \forall k \in \mathcal{K}$.

Proof: Please refer to [50] for the proof of the equivalency between problem $\mathcal{Q}_2^W$ and problem $\mathcal{Q}_3^W$.

When μ_k is large enough, we can obtain $\mathrm{Tr}\{\mathbf{\Gamma}_{T,k}\} \approx \lambda_{\max}\{\mathbf{\Gamma}_{T,k}\}$. However, the spectral function $\lambda_{\max}\{\mathbf{\Gamma}_{T,k}\}$ is not smooth (i.e., not differentiable). To proceed further, we use the subgradient of $\lambda_{\max}\{\mathbf{\Gamma}_{T,k}\}$ and have

$$\partial\lambda_{\max}\{\mathbf{\Gamma}_{T,k}\} = \mathbf{w}_{T,k,\max}\mathbf{w}_{T,k,\max}^H, \tag{15}$$

where $\mathbf{w}_{T,k,\max}$ is the eigenvector corresponding to the maximum eigenvalue of $\lambda_{\max}\{\mathbf{\Gamma}_{T,k}\}$. As such, it follows that

$$\lambda_{\max}\{\mathbf{\Gamma}\} - \lambda_{\max}\{\mathbf{\Gamma}_{T,k}\} \geq \left\langle \mathbf{w}_{T,k,\max}\mathbf{w}_{T,k,\max}^H, \mathbf{\Gamma} - \mathbf{\Gamma}_{T,k}\right\rangle, \forall \mathbf{\Gamma} \succeq 0. \tag{16}$$

Proposition 1: Given the initial weight coefficients μ_k and the initial feasible solution set $\mathbf{\Gamma}_T^{(0)}$, we can achieve the optimal solution to problem $\mathcal{Q}_3^W$ by solving the following problem $\mathcal{Q}^W$ iteratively.

$$\mathcal{Q}^W: \min_{\mathbf{\Gamma}_T} \sum_{k=1}^K \left\{(\mu_k + 1)\,\mathrm{Tr}\{\mathbf{\Gamma}_{T,k}\} - \mu_k\left\langle \mathbf{w}_{T,k,\max}^{(n-1)}\mathbf{w}_{T,k,\max}^{(n-1),H}, \mathbf{\Gamma}_{T,k}\right\rangle\right\} \tag{17a}$$

$$s.t.\ \mathrm{Tr}\left\{\tilde{\mathbf{h}}_{T,k}\tilde{\mathbf{h}}_{T,k}^H\left(\frac{1}{\gamma_k}\mathbf{\Gamma}_{T,k} - \sum_{\substack{m\in\mathcal{K},\\ m\neq k}}\mathbf{\Gamma}_{T,m}\right)\right\} - PJ_k \geq 0, \forall k \in \mathcal{K}, \tag{17b}$$

$$\mathbf{\Gamma}_{T,k} \succeq 0,\ \forall k \in \mathcal{K}, \tag{17c}$$

where the superscript $n{-}1$ is the $(n{-}1)$th iteration.

Proof: Please refer to Appendix A.

As a result, the optimal rank-one solution $\{\mathbf{\Gamma}_{T,k}\}$ to problem $\mathcal{Q}_2^W$ is achieved by using the proposition 1 [50]. Finally, the optimal $\{\mathbf{w}_{T,k}\}$ can be obtained from $\{\mathbf{\Gamma}_{T,k}\}$ by applying the eigenvalue decomposition.

C. Phase Shift Optimization with Probabilistic Constraints

For given transmit beamforming $\mathbf{W}_T$, the subproblem of phase shift $\mathbf{v}$ is simplified to a feasibility-check problem, which is recast as

$$\mathcal{Q}_1^V: \mathrm{Find}\quad \mathbf{v} \tag{18a}$$

$$s.t.\ \Pr_{\{\mathbf{H}_{J,k},\mathbf{h}_{J,k}\}}\left\{\tilde{\mathbf{h}}_{T,k}^H\boldsymbol{\xi}_{T,k}\tilde{\mathbf{h}}_{T,k} - J_k - \sigma_k^2 \geq 0\right\} \geq 1 - \rho_k, \forall k \in \mathcal{K}, \tag{18b}$$

$$|\mathrm{v}_n| = 1, \forall n, \tag{18c}$$

where $\boldsymbol{\xi}_{T,k} = \boldsymbol{\Gamma}_{T,k}/\gamma_k - \sum_{m\in\mathcal{K},m\neq k}^{K}\boldsymbol{\Gamma}_{T,m}$. Nevertheless, problem $\mathcal{Q}_1^V$ cannot be solved due to the following details. First, the configuration of $\mathbf{w}_J$ inside J_k is unknow. Second, the probabilistic constraints (18b) and unit-modulus constraints (18c) are concave. To make problem $\mathcal{Q}_1^V$ feasible, we first utilize the so-called use-and-then-forget method that is widely used in massive MIMO [32], i.e., $\mathbf{w}_J$ is known only during the process of solving $\mathcal{Q}_1^V$. Then, we apply Lemma 1 and 2 to convert (18b) into the SOCs or/and LMIs, and use the quadratic form to transform (18c) into a convex constraints. Finally, we obtain a relaxed and feasible problem by using the Cauchy-Schwarz inequality to address the unknown $\mathbf{w}_J$. As such, we can utilize the penalty non-smooth optimization method and CVX tool [54] to solve problem $\mathcal{Q}_1^V$ efficiently.

Before applying the lemmas to approximate the probabilistic constrains, (18b) should be transformed into a standard quadratic form $\Pr\left\{\mathbf{e}^H\mathbf{Q}\mathbf{e}+2\mathrm{Re}\left\{\mathbf{r}^H\mathbf{e}\right\}+s\geq 0\right\}$. By introducing the statistical CSI error into J_k and defining $\boldsymbol{\Gamma}_J=\mathbf{w}_J\mathbf{w}_J^H$, (18b) is then rewritten in (19) at the top of the next page. For the convenience of derivations, it is assumed that $\boldsymbol{\Sigma}_{HJ,k}=\varepsilon_{HJ,k}^2\mathbf{I}$ and $\boldsymbol{\Sigma}_{hJ,k}=\varepsilon_{hJ,k}^2\mathbf{I}$, then we have $\mathrm{vec}\left(\Delta\mathbf{H}_{J,k}\right)=\varepsilon_{HJ,k}\mathbf{e}_{HJ,k}$ and $\Delta\mathbf{h}_{J,k}=\varepsilon_{hJ,k}\mathbf{e}_{hJ,k}$ where $\mathbf{e}_{HJ,k},\mathbf{e}_{hJ,k}\sim\mathcal{CN}(0,\mathbf{I})$. For the first term ζ_1 inside (19), by applying mathematical transformations, ζ_1 is then rewritten as

$$\begin{aligned}\zeta_1=&\Delta\mathbf{h}_{J,k}^H\left(-\boldsymbol{\Gamma}_J\right)\Delta\mathbf{h}_{J,k}+2\mathrm{Re}\left\{\mathbf{v}^H\Delta\mathbf{H}_{J,k}\left(-\boldsymbol{\Gamma}_J\right)\Delta\mathbf{h}_{J,k}\right\}\\&+\mathbf{v}^H\Delta\mathbf{H}_{J,k}\left(-\boldsymbol{\Gamma}_J\right)\Delta\mathbf{H}_{J,k}^H\mathbf{v}\\=&\varepsilon_{hJ,k}^2\mathbf{e}_{hJ,k}^H\left(-\boldsymbol{\Gamma}_J\right)\mathbf{e}_{hJ,k}\\&+2\mathrm{Re}\left\{\mathrm{vec}\left(\Delta\mathbf{H}_{J,k}\right)\left(\mathbf{v}^*\otimes\left(-\boldsymbol{\Gamma}_J\right)\right)\Delta\mathbf{h}_{J,k}^*\right\}\\&+\mathrm{vec}\left(\Delta\mathbf{H}_{J,k}\right)\left(\mathbf{V}^T\otimes\left(-\boldsymbol{\Gamma}_J\right)\right)\mathrm{vec}^*\left(\Delta\mathbf{H}_{J,k}\right)\\=&-\varepsilon_{hJ,k}^2\mathbf{e}_{hJ,k}^H\boldsymbol{\Gamma}_J\mathbf{e}_{hJ,k}-\varepsilon_{HJ,k}^2\mathbf{e}_{HJ,k}\left(\mathbf{V}^T\otimes\boldsymbol{\Gamma}_J\right)\mathbf{e}_{HJ,k}^*\\&-2\mathrm{Re}\left\{\varepsilon_{HJ,k}\varepsilon_{hJ,k}\mathbf{e}_{HJ,k}^*\left(\mathbf{v}^*\otimes\boldsymbol{\Gamma}_J\right)\mathbf{e}_{hJ,k}^H\right\}\\=&\mathbf{e}_k^H\mathbf{Q}_k\mathbf{e}_k,\end{aligned}\tag{20}$$

where $\mathbf{e}_k=[\mathbf{e}_{hJ,k}^H,\mathbf{e}_{HJ,k}^T]^H$, $\mathbf{V}=\mathbf{v}\mathbf{v}^H$ and

$$\mathbf{Q}_k=-\begin{bmatrix}\boldsymbol{\Sigma}_{hJ,k}^{1/2}\boldsymbol{\Gamma}_J\boldsymbol{\Sigma}_{hJ,k}^{1/2} & \varepsilon_{HJ,k}\varepsilon_{hJ,k}\left(\mathbf{v}^*\otimes\boldsymbol{\Gamma}_J\right)\\ \varepsilon_{HJ,k}\varepsilon_{hJ,k}\left(\mathbf{v}^T\otimes\boldsymbol{\Gamma}_J\right) & \varepsilon_{HJ,k}^2\left(\mathbf{V}^T\otimes\boldsymbol{\Gamma}_J\right)\end{bmatrix}.$$

Proof: Please refer to Appendix B for detailed derivations of (20).

Next, the second term ζ_2 inside (19) is reformulated as

$$\begin{aligned}\zeta_2=&-2\mathrm{Re}\left\{\left(\widehat{\mathbf{h}}_{J,k}^H+\mathbf{v}^H\widehat{\mathbf{H}}_{J,k}\right)\boldsymbol{\Gamma}_J\Delta\mathbf{h}_{J,k}\right.\\&\left.+\left(\widehat{\mathbf{h}}_{J,k}^H+\mathbf{v}^H\widehat{\mathbf{H}}_{J,k}\right)\boldsymbol{\Gamma}_J\Delta\mathbf{H}_{J,k}^H\mathbf{v}\right\}\\=&-2\mathrm{Re}\left\{\left(\widehat{\mathbf{h}}_{J,k}^H+\mathbf{v}^H\widehat{\mathbf{H}}_{J,k}\right)\boldsymbol{\Gamma}_J\Delta\mathbf{h}_{J,k}\right.\\&\left.+\mathrm{vec}^T\left(\mathbf{v}\left(\widehat{\mathbf{h}}_{J,k}^H+\mathbf{v}^H\widehat{\mathbf{H}}_{J,k}\right)\boldsymbol{\Gamma}_J\right)\mathrm{vec}^*\left(\Delta\mathbf{H}_{J,k}\right)\right\}\\=&-2\mathrm{Re}\left\{\varepsilon_{hJ,k}\left(\widehat{\mathbf{h}}_{J,k}^H+\mathbf{v}^H\widehat{\mathbf{H}}_{J,k}\right)\boldsymbol{\Gamma}_J\mathbf{e}_{hJ,k}\right.\\&\left.+\varepsilon_{HJ,k}\mathrm{vec}^T\left(\mathbf{v}\left(\widehat{\mathbf{h}}_{J,k}^H+\mathbf{v}^H\widehat{\mathbf{H}}_{J,k}\right)\boldsymbol{\Gamma}_J\right)\mathbf{e}_{HJ,k}^*\right\}\\=&2\mathrm{Re}\left\{\mathbf{r}_k^H\mathbf{e}_k\right\},\end{aligned}\tag{21}$$

where

$$\mathbf{r}_k=-\begin{bmatrix}\varepsilon_{hJ,k}\boldsymbol{\Gamma}_J\left(\widehat{\mathbf{h}}_{J,k}+\widehat{\mathbf{H}}_{J,k}^H\mathbf{v}\right)\\ \varepsilon_{HJ,k}\mathrm{vec}^*\left(\mathbf{v}\left(\widehat{\mathbf{h}}_{J,k}^H+\mathbf{v}^H\widehat{\mathbf{H}}_{J,k}\right)\boldsymbol{\Gamma}_J\right)\end{bmatrix}.$$

Therefore, the outage constrains (18b) is equivalent to a standard quadratic form, which is given by

$$\Pr\left\{\mathbf{e}_k^H\mathbf{Q}_k\mathbf{e}_k+2\mathrm{Re}\left\{\mathbf{r}_k^H\mathbf{e}_k\right\}+s_k\geq 0\right\}\geq 1-\rho_k,\tag{22}$$

where

$$\begin{aligned}s_k=&\left(\widehat{\mathbf{h}}_{J,k}^H+\mathbf{v}^H\widehat{\mathbf{H}}_{J,k}\right)\left(-\boldsymbol{\Gamma}_J\right)\left(\widehat{\mathbf{h}}_{J,k}+\widehat{\mathbf{H}}_{J,k}^H\mathbf{v}\right)\\&+\left(\mathbf{h}_{T,k}^H+\mathbf{v}^H\mathbf{H}_{T,k}\right)\boldsymbol{\xi}_{T,k}\left(\mathbf{h}_{T,k}+\mathbf{H}_{T,k}^H\mathbf{v}\right)-\sigma^2.\end{aligned}$$

Applying Lemma 1 and 2[7], the approximation of outage constraints (18b) is given, respectively, as

$$\mathcal{A}_D:\mathrm{Tr}\left\{\mathbf{Q}_k\right\}-2\sqrt{\ln\left(1/\rho_k\right)}\left(x_k+y_k\right)+s_k\geq 0,\tag{23a}$$

$$\frac{1}{\sqrt{2}}\left\|\mathbf{r}_k\right\|\leq x_k,\tag{23b}$$

$$\beta_k\left\|\mathbf{Q}_k\right\|_F\leq y_k,\tag{23c}$$

$$\left(1-1/\left(2{\beta_k}^2\right)\right)\beta_k=\sqrt{\ln\left(1/\rho_k\right)},\tag{23d}$$

and

$$\mathcal{A}_B:\mathrm{Tr}\{\mathbf{Q}_k\}-\sqrt{2\ln\left(1/\rho_k\right)}x_k+\ln\left(\rho_k\right)y_k+s_k\geq 0,\tag{24a}$$

$$\sqrt{\left\|\mathbf{Q}_k\right\|_F^2+2\left\|\mathbf{r}_k\right\|_2^2}\leq x_k,\tag{24b}$$

$$y_k\mathbf{I}+\mathbf{Q}_k\succeq 0, y_k\geq 0,\tag{24c}$$

where $\mathcal{A}_D$ and $\mathcal{A}_B$ denote the DBLDI-based approximation and BTI-based approximation, respectively. x_k and y_k are the slack variables.

According to (49) in [34], we simplify $\mathrm{Tr}\left\{\mathbf{Q}_k\right\}$, $\left\|\mathbf{r}_k\right\|_2$, and $\left\|\mathbf{Q}_k\right\|_F$ as follows:

$$\begin{aligned}\mathrm{Tr}\left\{\mathbf{Q}_k\right\}=&-\mathrm{Tr}\left\{\left[\varepsilon_{hJ,k}\boldsymbol{\Gamma}_J^{1/2}\ \ \varepsilon_{HJ,k}\left(\mathbf{v}^*\otimes\boldsymbol{\Gamma}_J^{1/2}\right)\right]\right.\\&\left.\bullet\begin{bmatrix}\varepsilon_{hJ,k}\boldsymbol{\Gamma}_J^{1/2}\\ \varepsilon_{HJ,k}\left(\mathbf{v}^T\otimes\boldsymbol{\Gamma}_J^{1/2}\right)\end{bmatrix}\right\}\\=&-\varepsilon_{hJ,k}^2\mathrm{Tr}\left\{\boldsymbol{\Gamma}_J\right\}-\varepsilon_{HJ,k}^2\mathrm{Tr}\left(\mathbf{V}\right)\mathrm{Tr}\left(\boldsymbol{\Gamma}_J\right)\\=&-\left(\varepsilon_{hJ,k}^2+\varepsilon_{HJ,k}^2N\right)\mathrm{Tr}\left\{\boldsymbol{\Gamma}_J\right\},\end{aligned}\tag{25a}$$

$$\begin{aligned}\left\|\mathbf{r}_k\right\|_2^2=&\left\|\varepsilon_{hJ,k}\left(\widehat{\mathbf{h}}_{J,k}^H+\mathbf{v}^H\widehat{\mathbf{H}}_{J,k}\right)\boldsymbol{\Gamma}_J\right\|_2^2\\&+\left\|\varepsilon_{HJ,k}\mathrm{vec}^*\left(\mathbf{v}\left(\widehat{\mathbf{h}}_{J,k}^H+\mathbf{v}^H\widehat{\mathbf{H}}_{J,k}\right)\boldsymbol{\Gamma}_J\right)\right\|_2^2\\=&\left(\varepsilon_{hJ,k}^2+\varepsilon_{HJ,k}^2N\right)\left\|\left(\widehat{\mathbf{h}}_{J,k}^H+\mathbf{v}^H\widehat{\mathbf{H}}_{J,k}\right)\boldsymbol{\Gamma}_J\right\|_2^2,\end{aligned}\tag{25b}$$

$$\begin{aligned}\left\|\mathbf{Q}_k\right\|_F^2=&\varepsilon_{hJ,k}^4\left\|\boldsymbol{\Gamma}_J\right\|_F^2+\varepsilon_{HJ,k}^4\left\|\mathbf{V}^T\right\|_F^2\left\|\boldsymbol{\Gamma}_J\right\|_F^2\\&+2\left(\varepsilon_{HJ,k}\varepsilon_{hJ,k}\right)^2\left\|\mathbf{v}^*\right\|_F^2\left\|\boldsymbol{\Gamma}_J\right\|_F^2\\=&\left(\varepsilon_{hJ,k}^2+\varepsilon_{HJ,k}^2N\right)^2\left\|\boldsymbol{\Gamma}_J\right\|_F^2.\end{aligned}\tag{25c}$$

[7]Although similar BTI-based method has been employed in [34], the solution in [34] is not applicable to this paper which mainly focuses on the anti-jamming communication. We will evaluate the performance of BTI in the section VI.

$$\Pr_{\{\mathbf{H}_{J,k},\mathbf{h}_{J,k}\}}\left\{-J_k+\underbrace{\tilde{\mathbf{h}}_{T,k}^H\boldsymbol{\xi}_{t,k}\tilde{\mathbf{h}}_{T,k}-\sigma_k^2}_{\hat{s}_k}\geq 0\right\}=\Pr\left\{\left(\mathbf{h}_{J,k}^H+\mathbf{v}^H\mathbf{H}_{J,k}\right)\left(-\boldsymbol{\Gamma}_J\right)\left(\mathbf{h}_{J,k}^H+\mathbf{H}_{J,k}^H\mathbf{v}\right)+\hat{s}_k\geq 0\right\}$$

$$=\Pr\left\{\left(\left(\widehat{\mathbf{h}}_{J,k}+\Delta\mathbf{h}_{J,k}\right)^H+\mathbf{v}^H\left(\widehat{\mathbf{H}}_{J,k}+\Delta\mathbf{H}_{J,k}\right)\right)\left(-\boldsymbol{\Gamma}_J\right)\left(\left(\widehat{\mathbf{h}}_{J,k}+\Delta\mathbf{h}_{J,k}\right)+\left(\widehat{\mathbf{H}}_{J,k}^H+\Delta\mathbf{H}_{J,k}^H\right)\mathbf{v}\right)+\hat{s}_k\geq 0\right\}$$

$$=\Pr\left\{\underbrace{\left(\Delta\mathbf{h}_{J,k}^H+\mathbf{v}^H\Delta\mathbf{H}_{J,k}\right)\left(-\boldsymbol{\Gamma}_J\right)\left(\Delta\mathbf{h}_{J,k}+\Delta\mathbf{H}_{J,k}^H\mathbf{v}\right)}_{\zeta_1}+\underbrace{2\mathrm{Re}\left\{\left(\widehat{\mathbf{h}}_{J,k}^H+\mathbf{v}^H\widehat{\mathbf{H}}_{J,k}\right)\left(-\boldsymbol{\Gamma}_J\right)\left(\Delta\mathbf{h}_{J,k}+\Delta\mathbf{H}_{J,k}^H\mathbf{v}\right)\right\}}_{\zeta_2}\right.$$

$$\left.+\underbrace{\left(\widehat{\mathbf{h}}_{J,k}^H+\mathbf{v}^H\widehat{\mathbf{H}}_{J,k}\right)\left(-\boldsymbol{\Gamma}_J\right)\left(\widehat{\mathbf{h}}_{J,k}+\widehat{\mathbf{H}}_{J,k}^H\mathbf{v}\right)+\hat{s}_k}_{s_k}\geq 0\right\}. \tag{19}$$

Problem $\mathcal{Q}_1^V$ is then reformulated, respectively, for DBLDI-based approximation and BTI-based approximation, as

$$\mathcal{Q}_D^{V1}:\text{Find}\quad \mathbf{v},\mathbf{x},\mathbf{y}$$
$$s.t.\ -\left(\varepsilon_{h_{J,k}}^2+\varepsilon_{H_{J,k}}^2N\right)\mathrm{Tr}\left\{\boldsymbol{\Gamma}_J\right\}-2\sqrt{\ln\left(1/\rho_k\right)}(x_k+y_k)+s_k\geq 0,\forall k\in\mathcal{K}, \tag{26a}$$
$$\sqrt{\left(\varepsilon_{h_{J,k}}^2+\varepsilon_{H_{J,k}}^2N\right)}\left\|\left(\widehat{\mathbf{h}}_{J,k}^H+\mathbf{v}^H\widehat{\mathbf{H}}_{J,k}\right)\boldsymbol{\Gamma}_J\right\|_2\leq\sqrt{2}x_k\quad\forall k\in\mathcal{K}, \tag{26b}$$
$$\beta_k\left(\varepsilon_{h_{J,k}}^2+\varepsilon_{H_{J,k}}^2N\right)\left\|\boldsymbol{\Gamma}_J\right\|_F\leq y_k,\quad\forall k\in\mathcal{K}, \tag{26c}$$
$$|\mathrm{v}_n|=1,\forall n, \tag{26d}$$

where $\left(1-1/\left(2{\beta_k}^2\right)\right)\beta_k=\sqrt{\ln\left(1/\rho_k\right)}$, and

$$\mathcal{Q}_B^{V1}:\text{Find}\quad \mathbf{v},\mathbf{x}$$
$$s.t.\ -\left(\varepsilon_{h_{J,k}}^2+\varepsilon_{H_{J,k}}^2N\right)\mathrm{Tr}\left\{\boldsymbol{\Gamma}_J\right\}-\sqrt{2\ln\left(1/\rho_k\right)}x_k+\ln\left(\rho_k\right)y_k+s_k\geq 0,\forall k\in\mathcal{K}, \tag{27a}$$
$$\left\|\begin{array}{c}\left(\varepsilon_{h_{J,k}}^2+\varepsilon_{H_{J,k}}^2N\right)\mathrm{vec}\left(\boldsymbol{\Gamma}_J\right)\\ \sqrt{2\left(\varepsilon_{h_{J,k}}^2+\varepsilon_{H_{J,k}}^2N\right)}\left(\widehat{\mathbf{h}}_{J,k}^H+\mathbf{v}^H\widehat{\mathbf{H}}_{J,k}\right)\boldsymbol{\Gamma}_J\end{array}\right\|_2\leq x_k\quad\forall k\in\mathcal{K}, \tag{27b}$$
$$|\mathrm{v}_n|=1,\forall n, \tag{27c}$$

where $y_k=\lambda_{\max}^+\left(\left(\varepsilon_{h_{J,k}}^2+\varepsilon_{H_{J,k}}^2N\right)\boldsymbol{\Gamma}_j\right)$ in problem $\mathcal{Q}_B^{V1}$.

However, due to the unknown $\mathbf{w}_J$ and the non-convexity of constraints, the problem $\mathcal{Q}_D^{V1}$ and $\mathcal{Q}_B^{V1}$ are still unsolved. Inspired by [32], we first utilize the Cauchy-Schwarz inequality to obtain the bound of constraints, such that the problem's infeasiblity caused by the unknown $\mathbf{w}_J$ can be addressed. Specifically, the bound of s_k, constraints (26b) , and constraints (27b) are given by

$$s_k=\left(\mathbf{h}_{J,k}^H+\mathbf{v}^H\widehat{\mathbf{H}}_{J,k}\right)\left(-\boldsymbol{\Gamma}_J\right)\left(\mathbf{h}_{J,k}+\widehat{\mathbf{H}}_{J,k}^H\mathbf{v}\right)+\hat{s}_k$$
$$=-\left|\left(\mathbf{h}_{J,k}^H+\mathbf{v}^H\widehat{\mathbf{H}}_{J,k}\right)\mathbf{w}_J\right|^2+\hat{s}_k$$
$$\geq -P_J\left\|\mathbf{h}_{J,k}^H+\mathbf{v}^H\widehat{\mathbf{H}}_{J,k}\right\|_2^2+\hat{s}_k \tag{28a}$$

$$\sqrt{\left(\varepsilon_{h_{J,k}}^2+\varepsilon_{H_{J,k}}^2N\right)}\left\|\left(\widehat{\mathbf{h}}_{J,k}^H+\mathbf{v}^H\widehat{\mathbf{H}}_{J,k}\right)\boldsymbol{\Gamma}_J\right\|_2$$
$$\leq\sqrt{\left(\varepsilon_{h_{J,k}}^2+\varepsilon_{H_{J,k}}^2N\right)}\left\|\boldsymbol{\Gamma}_J\right\|_F\left\|\widehat{\mathbf{h}}_{J,k}^H+\mathbf{v}^H\widehat{\mathbf{H}}_{J,k}\right\|_2$$
$$=P_J\sqrt{\left(\varepsilon_{h_{J,k}}^2+\varepsilon_{H_{J,k}}^2N\right)}\left\|\widehat{\mathbf{h}}_{J,k}^H+\mathbf{v}^H\widehat{\mathbf{H}}_{J,k}\right\|_2, \tag{28b}$$
$$\left\|\begin{array}{c}\left(\varepsilon_{h_{J,k}}^2+\varepsilon_{H_{J,k}}^2N\right)\mathrm{vec}\left(\boldsymbol{\Gamma}_J\right)\\ \sqrt{2\left(\varepsilon_{h_{J,k}}^2+\varepsilon_{H_{J,k}}^2N\right)}\left(\widehat{\mathbf{h}}_{J,k}^H+\mathbf{v}^H\widehat{\mathbf{H}}_{J,k}\right)\boldsymbol{\Gamma}_J\end{array}\right\|_2^2$$
$$=\left\|\sqrt{2\left(\varepsilon_{h_{J,k}}^2+\varepsilon_{H_{J,k}}^2N\right)}\left(\widehat{\mathbf{h}}_{J,k}^H+\mathbf{v}^H\widehat{\mathbf{H}}_{J,k}\right)\boldsymbol{\Gamma}_J\right\|_2^2$$
$$+\left\|\left(\varepsilon_{h_{J,k}}^2+\varepsilon_{H_{J,k}}^2N\right)\boldsymbol{\Gamma}_J\right\|_F^2\leq P_J^2\left(\varepsilon_{h_{J,k}}^2+\varepsilon_{H_{J,k}}^2N\right)^2$$
$$+P_J^2\left\|\sqrt{2\left(\varepsilon_{h_{J,k}}^2+\varepsilon_{H_{J,k}}^2N\right)}\left(\widehat{\mathbf{h}}_{J,k}^H+\mathbf{v}^H\widehat{\mathbf{H}}_{J,k}\right)\right\|_2^2, \tag{28c}$$

where P_J denotes the power value of $\|\mathbf{w}_J\|_2^2$, which can be obtained by using the signal strength and channel gains [32], [48]. However, owing to the CSI uncertainties of jammer's channels caused by the uplink-downlink channel reciprocity mismatch [55], [56], P_J can not be accurately acquired. Following [57], we adopt $\left|P_J-\widehat{P}_J\right|/P_J\leq\varepsilon_{PJ}$ to denote the estimation error of $\|\mathbf{w}_J\|_2^2$, where $\widehat{P}_J$ is the estimation value. As such, combining with the fact $\mathrm{Tr}\left\{\boldsymbol{\Gamma}_J\right\}=\left\|\boldsymbol{\Gamma}_J\right\|_F=P_J$, the problem $\mathcal{Q}_D^{V1}$ and $\mathcal{Q}_B^{V1}$ can be reformulated as the worst-case problems, i.e.,

$$\mathcal{Q}_D^{V2}:\text{Find}\quad \mathbf{v},\mathbf{x},\mathbf{y}$$
$$s.t.\ -\widetilde{P}_J\left(\varepsilon_{h_{J,k}}^2+\varepsilon_{H_{J,k}}^2N\right)-2\sqrt{\ln\left(1/\rho_k\right)}(x_k+y_k)+\widetilde{s}_k\geq 0,\forall k\in\mathcal{K}, \tag{29a}$$
$$\widetilde{P}_J\sqrt{\left(\varepsilon_{h_{J,k}}^2+\varepsilon_{H_{J,k}}^2N\right)}\left\|\widehat{\mathbf{h}}_{J,k}^H+\mathbf{v}^H\widehat{\mathbf{H}}_{J,k}\right\|_2\leq\sqrt{2}x_k\quad\forall k\in\mathcal{K}, \tag{29b}$$
$$\beta_k\widetilde{P}_J\left(\varepsilon_{h_{J,k}}^2+\varepsilon_{H_{J,k}}^2N\right)\leq y_k,\quad\forall k\in\mathcal{K}, \tag{29c}$$
$$|\mathrm{v}_n|=1,\forall n, \tag{29d}$$

and

$$\mathcal{Q}_B^{V2}: \text{Find} \quad \mathbf{v}, \mathbf{x}$$
$$s.t. \; -\widetilde{P}_J\left(\varepsilon_{h_{J,k}}^2+\varepsilon_{H_{J,k}}^2 N\right)-\sqrt{2\ln(1/\rho_k)}x_k + \ln(\rho_k)\, y_k + \widetilde{s}_k \geq 0, \forall k \in \mathcal{K}, \quad (30a)$$
$$\left(\widetilde{P}_J\left\|\sqrt{2\left(\varepsilon_{h_{J,k}}^2+\varepsilon_{H_{J,k}}^2 N\right)}\left(\widehat{\mathbf{h}}_{J,k}^H+\mathbf{v}^H\widehat{\mathbf{H}}_{J,k}\right)\right\|_2\right)^2 + \left(\widetilde{P}_J\left(\varepsilon_{h_{J,k}}^2+\varepsilon_{H_{J,k}}^2 N\right)\right)^2 \leq x_k^2, \quad \forall k \in \mathcal{K}, \quad (30b)$$
$$|\mathrm{v}_n| = 1, \forall n, \quad (30c)$$

where $\widetilde{s}_k = -\widetilde{P}_J\left\|\mathbf{h}_{J,k}^H+\mathbf{v}^H\widehat{\mathbf{H}}_{J,k}\right\|_2^2+\widehat{s}_k$, and $\widetilde{P}_J = \widehat{P}_J\big/(1-\varepsilon_{PJ})$. Although this operation leads to a suboptimal solution, from a practical implementation point of view, a tradeoff should be made between the feasibility and optimality[8].

Then, we introduce two auxiliary matrixes and an auxiliary vector to deal with the non-convexity of constraints induced by $\mathbf{v}$, which are expressed as

$$\mathbf{R}_k = \begin{bmatrix} \mathbf{H}_{T,k}\boldsymbol{\xi}_{T,k}\mathbf{H}_{T,k}^H - \widetilde{P}_J\widehat{\mathbf{H}}_{J,k}\widehat{\mathbf{H}}_{J,k}^H & \widetilde{\mathbf{R}}_k \\ \widetilde{\mathbf{R}}_k^H & 0 \end{bmatrix}, \quad (31a)$$

$$\mathbf{C}_{J,k} = \widetilde{P}_J^2 \begin{bmatrix} \widehat{\mathbf{H}}_{J,k}\widehat{\mathbf{H}}_{J,k}^H & \widehat{\mathbf{H}}_{J,k}\mathbf{h}_{J,k} \\ \left(\widehat{\mathbf{H}}_{J,k}\mathbf{h}_{J,k}\right)^H & \left\|\mathbf{h}_{J,k}^H\right\|_2^2 \end{bmatrix}, \widehat{\mathbf{v}} = \begin{bmatrix} \mathbf{v} \\ 1 \end{bmatrix} \quad (31b)$$

where $\widetilde{\mathbf{R}}_k = \mathbf{H}_{T,k}\boldsymbol{\xi}_{T,k}\mathbf{h}_{T,k} - \widetilde{P}_J\widehat{\mathbf{H}}_{J,k}\widehat{\mathbf{h}}_{J,k}$. With $\mathbf{R}_k$, $\mathbf{C}_{J,k}$ and $\mathbf{v}$, s_k and $\|\mathbf{r}_k\|_2^2$ are modified as follows:

$$s_k^{\widehat{V}} = \mathrm{Tr}\left\{\mathbf{R}_k\widehat{\mathbf{V}}\right\} + \mathbf{h}_{T,k}^H\boldsymbol{\xi}_{T,k}\mathbf{h}_{T,k} - \widetilde{P}_J\mathbf{h}_{J,k}^H\mathbf{h}_{J,k} - \sigma_k^2, \quad (32)$$

$$\left(\|\mathbf{r}_k\|_2^2\right)^{\widehat{V}} = \left(\varepsilon_{h_{J,k}}^2+\varepsilon_{H_{J,k}}^2 N\right)\mathrm{Tr}\left\{\mathbf{C}_{J,k}\widehat{\mathbf{V}}\right\}, \widehat{\mathbf{V}} = \widehat{\mathbf{v}}\widehat{\mathbf{v}}^H \quad (33)$$

In order to obtain better converged solution of $\mathbf{v}$, we further introduce slack variables $\boldsymbol{\alpha} = \{\alpha_1, \alpha_2, \cdots, \alpha_K\}^T$ into (29a) and (30a), which enforces outage probability to be larger than the target so that the transmit power is reduced [23]. Accordingly, $\mathcal{Q}_D^{V2}$ and $\mathcal{Q}_B^{V2}$ are respectively reformulated as

$$\mathcal{Q}_D^{V3}: \max_{\widehat{\mathbf{V}},\mathbf{x},\mathbf{y},\boldsymbol{\alpha}} \sum_{k=1}^K \alpha_k$$
$$s.t. \; -\widetilde{P}_J\left(\varepsilon_{h_{J,k}}^2+\varepsilon_{H_{J,k}}^2 N\right)-2\sqrt{\ln(1/\rho_k)}(x_k+y_k) + s_k^{\widehat{V}} - \alpha_k \geq 0, \forall k \in \mathcal{K}, \quad (34a)$$
$$\left(\|\mathbf{r}_k\|_2^2\right)^{\widehat{V}} - \left(4\mathrm{Re}\left\{x_k^{(n-1)}x_k\right\} - 2x_k^{(n-1),2}\right) \leq 0 \quad \forall k \in \mathcal{K}, \quad (34b)$$
$$\beta_k^2\widetilde{P}_J^2\left(\varepsilon_{h_{J,k}}^2+\varepsilon_{H_{J,k}}^2 N\right)^2 - \left(2\mathrm{Re}\left\{y_k^{(n-1)}y_k\right\} - y_k^{(n-1),2}\right) \leq 0, \forall k \in \mathcal{K}, \quad (34c)$$

[8]Since the impact of power estimation error on the system performance has been widely investigated in [13] and [58], this paper fixed $\varepsilon_{PJ} = 0.1$ in the original paper for simplicity. As for the practical issuses that the uplink-downlink channel reciprocity mismatch, the impact analysis and calibration have been investigated in [55] and [56], and the full characterization of this case in our model requires a full journal paper to be conceived in our future research.

Algorithm 1: DBLDI (BTI)-based Alternative Optimization (AO) Algorithm.

Input: $\left\{\mathbf{h}_{T,k}, \widehat{\mathbf{h}}_{J,k}, \mathbf{H}_{T,k}, \widehat{\mathbf{H}}_{J,k}, \gamma_k, \widetilde{P}_J, \varepsilon_{hJ,k}, \varepsilon_{HJ,k}\right\}$ and $B = 50$.
Set the tolerance of accuracy $\epsilon_1 = 10^{-4}$ and $\epsilon_2 = 10^{-4}$;
Initialize the feasible solutions $\mathbf{v}^{(0)}$, $\epsilon^{(0)} = \epsilon_1$;
Set the iteration number $n_1 = 1$ and $n_2 = 1$;
while $\epsilon^{(n_1-1)} \geq \epsilon_1$ & $n_1 \leq B$ **do**
  Initialize $\left\{\mathbf{\Gamma}_{T,k}^{(n_2-1)}\right\}$ and $\mathbf{w}_{T,k,\max}^{(n_2-1)}$ corresponding to $\lambda_{\max}\left\{\mathbf{\Gamma}_{T,k}^{(n_2-1)}\right\}$;
  while $\mathrm{Tr}\left\{\mathbf{\Gamma}_{T,k}^{(n_2-1)}\right\} - \lambda_{\max}\left\{\mathbf{\Gamma}_{T,k}^{(n_2-1)}\right\} \geq \epsilon_2$ & $n_2 \leq B$ **do**
    Solve Problem $\mathcal{Q}^W$ with given $\mathbf{v}^{(n_1-1)}$ and obtain the solutions $\left\{\mathbf{\Gamma}_{T,k}^{(n_2)}\right\}$;
    if $\left\{\mathbf{\Gamma}_{T,k}^{(n_2)}\right\} \approx \left\{\mathbf{\Gamma}_{T,k}^{(n_2-1)}\right\}$ **then**
      $\mu_k = 2\mu_k$;
      else
        $n_2 = n_2 + 1$;
      end
    end
  end
  Extract $\mathbf{W}_T^{(n_1)}$ from $\mathbf{\Gamma}_T^{(n_2)}$ by using the eigenvalue decomposition, and set $n_2 = 1$;
  Compute $\mathbf{v}^{(n_1)}$ through $\mathcal{Q}_D^V$ ($\mathcal{Q}_B^V$) with similar procedure of *step* 5-15;
  Update $\epsilon^{(n_1)} = \left\|\mathbf{W}_T^{(n_1)}\right\|_F^2 - \left\|\mathbf{W}_T^{(n_1-1)}\right\|_F^2$;
  Set $n_1 = n_1 + 1$;
end
Output: Transmit beamforming $\mathbf{W}_T$ and phase shift $\mathbf{v}$.

$$\widehat{\mathbf{V}} \succeq 0, \left[\widehat{\mathbf{V}}\right]_{n,n} = 1, \forall n, \quad (34d)$$
$$\alpha_k \geq 0, \forall k \in \mathcal{K}, \quad (34e)$$
$$\mathrm{rank}\left(\widehat{\mathbf{V}}\right) = 1, \quad (34f)$$

and

$$\mathcal{Q}_B^{V3}: \max_{\widehat{\mathbf{V}},\mathbf{x},\boldsymbol{\alpha}} \sum_{k=1}^K \alpha_k$$
$$s.t. \; -\widetilde{P}_J\left(\varepsilon_{h_{J,k}}^2+\varepsilon_{H_{J,k}}^2 N\right)-\sqrt{2\ln(1/\rho_k)}x_k + \ln(\rho_k)\, y_k + s_k^{\widehat{V}} - \alpha_k \geq 0, \forall k \in \mathcal{K}, \quad (35a)$$
$$\left(\varepsilon_{h_{J,k}}^2+\varepsilon_{H_{J,k}}^2 N\right)^2\widetilde{P}_J^2 - \left(2\mathrm{Re}\left\{x_k^{(n-1)}x_k\right\} - x_k^{(n-1),2}\right) + 2\left(\|\mathbf{r}_k\|_2^2\right)^{\widehat{V}} \leq 0, \forall k \in \mathcal{K}, \quad (35b)$$
(34d), (34e), (34f),

where $x_k^{(n-1)}$ and $y_k^{(n-1)}$ are the optimal solution of the $(n-1)$th iteration. Similarly, we use penalty non-smooth optimization method to deal with the rank-one constraints (34f), which is given by

$$\mathrm{rank}\left(\widehat{\mathbf{V}}\right) = 1 \Rightarrow \mathrm{Tr}\left\{\widehat{\mathbf{V}}\right\} - \left\langle\widehat{\mathbf{v}}_{\max}^{(n-1)}\widehat{\mathbf{v}}_{\max}^{(n-1),H}, \widehat{\mathbf{V}}\right\rangle \leq \tau, \quad (36)$$

where $\mathbf{v}_{\max}^{(n-1)}$ is the eigenvector corresponding to the maximum eigenvalue of $\lambda_{\max}\left\{\mathbf{V}^{(n-1)}\right\}$, the superscript $n-1$ denotes the $(n$–$1)$th iteration, and $\tau > 0$ is a penalty parameter.

Proof: Please refer to Appendix C.

To this end, the phase shift optimization problem $\mathcal{Q}_1^V$ is reformulated, respectively, as

$$\mathcal{Q}_D^V: \max_{\widehat{\mathbf{V}},\mathbf{x},\mathbf{y},\boldsymbol{\alpha},\tau} \sum_{k=1}^{K}\alpha_k - \chi\tau \quad s.t.\ (34a),(34b),(34c),(34d),(34e),(36), \tag{37}$$

and

$$\mathcal{Q}_B^V: \max_{\widehat{\mathbf{V}},\mathbf{x},\boldsymbol{\alpha},\tau} \sum_{k=1}^{K}\alpha_k - \chi\tau \quad s.t.\ (35a),(35b),(34d),(34e),(36), \tag{38}$$

where χ is a weight coefficient. Problem $\mathcal{Q}_B^V$ and $\mathcal{Q}_D^V$ can be solved efficiently through CVX tool, and thus $\mathbf{v}$ is achieved from $\widehat{\mathbf{V}}$ by using eigenvalue decomposition.

In summary, we can obtain the optimal $\mathbf{W}_T$ and $\mathbf{v}$ by alternately using the approaches proposed in section III-B and III-C until convergence. Specifically, in each aspect of the proposed AO approach, an attentive solution to $\mathbf{W}_T$ and $\mathbf{v}$ can be obtained by iteratively solving $\mathcal{Q}^W$ and $\mathcal{Q}_D^V$ ($\mathcal{Q}_B^V$) until convergence, respectively. Then, under the AO framework, the whole iterative algorithm will converge to a stationary solution with satisfactory performance as in [23], [33], [39], [41]. The details of the proposed AO algorithms are summarized in Algorithm 1.

D. Convergence, Optimality, and Initial Point Analysis

In this section, we first analyse the convergence and the optimality of different aspects of the proposed approaches, and then that of whole AO algorithm has been presented. In addition, since a feasible initial point is required for $\mathcal{Q}^W$ and $\mathcal{Q}_D^V$ ($\mathcal{Q}_B^V$), we provided the initial point search algorithm.

First, the problem $\mathcal{F}$ can be divided into two subproblems, i.e., $\mathcal{Q}^W$ and $\mathcal{Q}_D^V$ ($\mathcal{Q}_B^V$), which is given by (17) and (37)((38)). Then, we analyse the convergence and the optimality of $\mathcal{Q}^W$ and $\mathcal{Q}_D^V$ ($\mathcal{Q}_B^V$), respectively. As for $\mathcal{Q}^W$, the relationship between nth and $(n-1)$th iteration can be derived, which is given by E.q. (A.3) in Appendix A. Evidently, we can achieve a better solution $\left\{\mathbf{\Gamma}_{T,k}^{(n)}\right\}$ by solving problem $\mathcal{Q}^W$ iteratively. To the end, since $\left\{\mathbf{\Gamma}_{T,k}^{(n)}\right\}$ are bounded by the constraint (17b), the solution $\left\{\mathbf{\Gamma}_{T,k}^{(n)}\right\}$ will converge to an attentive point, which is the optimality of $\mathcal{Q}^W$ in each iteration. Similarly, as for $\mathcal{Q}_D^V$ ($\mathcal{Q}_B^V$), through the substitution of (36) into the objective function of $\mathcal{Q}_D^V$ ($\mathcal{Q}_B^V$), the relationship between nth and $(n-1)$th iteration can be obtained, which are given by

$$\begin{aligned}
&\sum_{k=1}^{K}\alpha_k^{(n)} - \chi\left(\mathrm{Tr}\left\{\widehat{\mathbf{V}}^{(n)}\right\} - \lambda_{\max}\left\{\widehat{\mathbf{V}}^{(n)}\right\}\right)\\
&\geq \sum_{k=1}^{K}\alpha_k^{(n)} - \chi\left(\mathrm{Tr}\left\{\widehat{\mathbf{V}}^{(n)}\right\} - \lambda_{\max}\left\{\widehat{\mathbf{V}}^{(n-1)}\right\}\right.\\
&\qquad\left. - \left\langle \widehat{\mathbf{v}}_{\max}^{(n-1)}\widehat{\mathbf{v}}_{\max}^{(n-1),H}, \widehat{\mathbf{V}}^{(n)} - \widehat{\mathbf{V}}\right\rangle\right)\\
&\geq \sum_{k=1}^{K}\alpha_k^{(n-1)} - \chi\left(\mathrm{Tr}\left\{\widehat{\mathbf{V}}^{(n-1)}\right\} - \lambda_{\max}\left\{\widehat{\mathbf{V}}^{(n-1)}\right\}\right).
\end{aligned} \tag{39}$$

Obviously, a better solution $\mathbf{V}^{(n)}$ can be obtained by solving problem $\mathcal{Q}_D^V$ ($\mathcal{Q}_B^V$) iteratively. Then, since $\mathbf{V}^{(n)}$ is bounded by the constraints of $\mathcal{Q}_D^V$ ($\mathcal{Q}_B^V$), the solution $\mathbf{V}^{(n)}$ to $\mathcal{Q}_D^V$ ($\mathcal{Q}_B^V$) can also converge to an attentive point, which is the optimality of $\mathcal{Q}_D^V$ ($\mathcal{Q}_B^V$) in each iteration.

Then, we analyse the convergence and the optimality of whole AO algorithm. Since $\mathbf{W}_T$ and $\mathbf{v}$ are optimized in an iterative manner by using the proposed AO algorithm, we can obtain that [23]

$$P\left(\mathbf{W}_T^{(1)},\mathbf{v}^{(1)}\right) \geq P\left(\mathbf{W}_T^{(2)},\mathbf{v}^{(2)}\right) \geq \cdots \geq P\left(\mathbf{W}_T^{(n)},\mathbf{v}^{(n)}\right), \tag{40}$$

where $P(\mathbf{W}_T,\mathbf{v}) = \|\mathbf{W}_T\|_F^2$ denotes the objective value of problem $\mathcal{F}$. Since $\mathbf{W}_T$ are bounded by the constraint (17b) and $\mathbf{v}$ are bounded by the constraints (34a)-(34d), $P\left(\mathbf{W}_T^{(n)},\mathbf{v}^{(n)}\right)$ is guaranteed to converge to a stationary solution with satisfactory performance, which is regarded as the optimality of the AO approach. In addition, the convergence of proposed algorithms is illustrated in Fig. 3, which further demonstrates that the proposed algorithms can converge to a stationary solution with satisfactory performance.

Algorithm 2: Initial Point Search Algorithm.

Input: $\left\{\mathbf{h}_{T,k},\widehat{\mathbf{h}}_{J,k},\mathbf{H}_{T,k},\widehat{\mathbf{H}}_{J,k},\gamma_k,\widetilde{P}_J,\varepsilon_{hJ,k},\varepsilon_{HJ,k}\right\}$ and $B = 50$.

Set the tolerance of accuracy $\epsilon_3 = 10^{-4}$;
Initialize the algorithm with random points $\widehat{\mathbf{V}}^{(0)},\mathbf{x}^{(0)},\mathbf{y}^{(0)},\boldsymbol{\alpha}^{(0)}$, $\epsilon^{(0)} = \epsilon_3$;
Set the iteration number $n_3 = 1$;
while $\epsilon^{(n_3-1)} \geq \epsilon_3$ & $n_3 \leq B$ **do**
  Set $n_3 = n_3 + 1$;
  Solve the problem $\mathcal{Q}_{D\,\text{initial}}^V$ ($\mathcal{Q}_{B\,\text{initial}}^V$);
  Update $\widehat{\mathbf{V}}^{(n_3)},\mathbf{x}^{(n_3)},\mathbf{y}^{(n_3)},\boldsymbol{\alpha}^{(n_3)}$;
end
Set $n_3 = 1$;

Output: $\widehat{\mathbf{V}}^{(0)},\mathbf{x}^{(0)},\mathbf{y}^{(0)},\boldsymbol{\alpha}^{(0)}$.

Then, we provide the method for searching the feasible initial point of $\mathcal{Q}^W$ and $\mathcal{Q}_D^V$ ($\mathcal{Q}_B^V$). As in [23], [33], [39], we first utilize the random method to randomly generate the the initial points, which may results in low convergence rate and sometimes infeasibility [59]. Thus, accroding to [59], a low-complexity algorithm can be used to search for the initial points. Specifically, we introduce two positive variables δ_1 and δ_2 to measure how far the constraints of $\mathcal{Q}^W$ and $\mathcal{Q}_D^V$ ($\mathcal{Q}_B^V$)

are from being satisfied, respectively, and the initialization problems are

$$\mathcal{Q}^{W}_{\text{initial}}: \max_{\mathbf{\Gamma}_T} \delta_1 \quad s.t.\ (17b)^*, (17c), \tag{41}$$

and

$$\mathcal{Q}^{V}_{D\,\text{initial}}: \max_{\widehat{\mathbf{V}},\mathbf{x},\mathbf{y},\boldsymbol{\alpha},} \delta_2 \quad s.t.\ (34a)^*, (34b)^*, (34c)^*, (34d), (34e)^*, (36)^*, \tag{42}$$

$$\mathcal{Q}^{V}_{B\,\text{initial}}: \max_{\widehat{\mathbf{V}},\mathbf{x},\boldsymbol{\alpha},} \delta_2 \quad s.t.\ (35a)^*, (35b)^*, (34d), (34e)^*, (36)^*, \tag{43}$$

where the constraint $(X)^* \in \{\text{constraintsof } (X)\}$ corresponds to the modified version of (X) with δ_1 or δ_2. To obtain the constraints $(X)^*$, we first rewrite the constraint (X) as $f(x) \leq 0$, and then replace it with $f(x) \leq \delta_1$ or $f(x) \leq \delta_2$. Finally, the feasible initial points $\mathbf{\Gamma}_T^{(0)}$ can be obtained by directly solving $\mathcal{Q}^{W}_{\text{initial}}$, and $\widehat{\mathbf{V}}^{(0)}, \mathbf{x}^{(0)}, \mathbf{y}^{(0)}, \boldsymbol{\alpha}^{(0)}$ can be obtained by solving $\mathcal{Q}^{V}_{D\,\text{initial}}$ ($\mathcal{Q}^{V}_{B\,\text{initial}}$) based on the similar iterative approximation method, which is summarized in Algorithm 2.

IV. Practical Beamforming Design without Jammer's Information

In this section, we consider the fact that it may be difficult to obtain the jammer's CSI due to the lack of cooperation. To solve this problem, a low complexity beamforming design is proposed. Specifically, we divide the joint beamforming design into two subproblems, i.e. transmit beamforming optimization and phase shift design. For optimizing the transmit beamforming, we apply the proposed method in section III-B, since J_k can be regarded as a fixed jamming power in one iteration. In terms of phase shift design, we convert the feasibility-check problem into the weighted channel gain maximization problem. Then, under the AO framework, we can use the penalty non-smooth optimization method to solve this problem efficiently.

With the optimal transmit beamforming $\mathbf{W}_T$ obtained from section III-B, we try to optimize phase shift $\mathbf{v}$ under the case that jammer's CSI is unavailable. Our purpose is to constructively maximize the desired signal power and destructively decrease the jamming power. Thus, under the worst-case case that the jammer's CSI is completely unknown, we can only maximize the desired signal power for practical implementation [23]. Accordingly, the desired signal power maximization is equivalent to the combined channel gain maximization. Therefore, the subproblem corresponding to $\mathbf{v}$ can be rewritten as

$$\mathcal{Q}^{V1}_{P}: \max_{\mathbf{v}} \sum_{k=1}^{K} \left|(\mathbf{h}_{T,k}^H + \mathbf{v}^H\mathbf{H}_{T,k})\mathbf{w}_{T,k}\right|^2 \tag{44a}$$

$$s.t.\ \ |\mathrm{v}_n| = 1, \forall n. \tag{44b}$$

Note that the combined channel gain of each user is difficult to maximize at the same time, the phase shifts at the IRS have to be adjusted on a user basis. Thus, we adopt the weighted channel gain to replace the sum of the combined channel gain, which resolves the problem above. By introducing the weights $\frac{1}{\gamma_k P J_k}, \forall k \in \mathcal{K}$, problem $\mathcal{Q}^{V1}_{P}$ is transformed into

$$\mathcal{Q}^{V2}_{P}: \max_{\mathbf{v}} \sum_{k=1}^{K} \frac{1}{\gamma_k P J_k}\left|(\mathbf{h}_{T,k}^H + \mathbf{v}^H\mathbf{H}_{T,k})\mathbf{w}_{T,k}\right|^2 \tag{45a}$$

$$s.t.\ \ |\mathrm{v}_n| = 1, \forall n. \tag{45b}$$

It is observed that problem $\mathcal{Q}^{V2}_{P}$ is non-convex problem. Then, we expand (45a) as

$$\mathbf{v}^H\mathbf{H}_{T,k}\mathbf{H}_{T,k}^H\mathbf{v}+\mathbf{v}^H\mathbf{H}_{T,k}\mathbf{h}_{T,k}+\mathbf{h}_{T,k}^H\mathbf{H}_{T,k}^H\mathbf{v}+\left\|\mathbf{h}_{T,k}^H\right\|_2^2. \tag{46}$$

By introducing an auxiliary matrix $\mathbf{E}_{T,k}$, the problem $\mathcal{Q}^{V2}_{P}$ is equivalently written as

$$\mathcal{Q}^{V3}_{P}: \max_{\widehat{\mathbf{V}}} \sum_{k=1}^{K} \frac{1}{\gamma_k P J_k}\mathrm{Tr}\left\{\mathbf{E}_{t,k}\widehat{\mathbf{V}}\right\} \quad s.t.\ (34d), (34f), \tag{47}$$

where

$$\mathbf{E}_{T,k} = \begin{bmatrix} \mathbf{H}_{T,k}\mathbf{H}_{T,k}^H & \mathbf{H}_{T,k}\mathbf{h}_{T,k} \\ \mathbf{h}_{T,k}^H\mathbf{H}_{T,k}^H & \left\|\mathbf{h}_{T,k}^H\right\|^2 \end{bmatrix}$$

Next, (36) is applied to deal with (34f), and thus problem $\mathcal{Q}^{V3}_{P}$ is reformulated as

$$\mathcal{Q}^{V}_{P}: \max_{\widehat{\mathbf{V}},\tau} \sum_{k=1}^{K} \frac{1}{\gamma_k P J_k}\mathrm{Tr}\left\{\mathbf{E}_{t,k}\widehat{\mathbf{V}}\right\} - \chi\tau \quad s.t.\ (34d), (36). \tag{48}$$

As problem $\mathcal{Q}^{V}_{P}$ is a standard SDP, it can be optimally solved by CVX tool. Compared to the AO algorithm proposed in section III, the low complexity algorithm has lower computational complexity and better convergence performance, which will be analyzed in the following sections. However, it may lead to a suboptimal solution, which will be subsequently presented in the section VI. In addition, the convergence and the optimality of the proposed practical scheme can be proved, which is similar to Section III-D and omitted here for simplicity.

V. Computational Complexity Analysis

In this section, the computational complexities of the proposed algorithms are analyzed in details. Since the three convex formulations only involve LMI and SOC constraints, they can be solved by a standard interior point methods (IPMs) [49]. According to [49], the worst-case runtime is used to compare the computational complexitiy, which can be expressed as

$$\mathcal{O}\left(n\sqrt{\sum_{j=1}^{p}\alpha_j + 2\kappa}\left(\underbrace{\sum_{j=1}^{p}\alpha_j^3 + n\sum_{j=1}^{p}\alpha_j^2}_{\text{due to LMI}} + \underbrace{n\sum_{i=1}^{m}\xi_i^2}_{\text{due to SOC}} + n^2\right)\right),$$

where n is the number of variables, p is the number of LMI of size α_j, and κ is the number of SOC of size ξ_i. Thus, the computational complexities of the proposed algorithms are presented as follows:

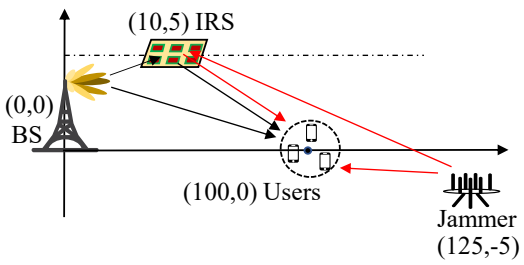

Fig. 2: Simulation deployment.

- *DBLDI-based AO algorithm:* The complexity of DBLDI-based AO per iteration contains two parts, i.e. the transmit beamforming part $o_{\mathbf{W}_T}$ and phase shift part $o_{\mathbf{\Phi}-\mathrm{DBLDI}}$. For the transmit beamforming, the complexity of problem $\mathcal{Q}^W$ is $o_{\mathbf{W}_T} = \mathcal{O}\Big(n_1\sqrt{K\left(M+1\right)}\left(K\left(M^3+1\right)+n_1K\left(M^2+1\right)+n_1^2\right)\Big)$ where $n_1 = \mathcal{O}\left(KM^2\right)$. In terms of phase shift, the complexity of problem $\mathcal{Q}_D^V$ is $o_{\mathbf{\Phi}-\mathrm{DBLDI}} = \mathcal{O}\Big(n_2\sqrt{N+1+8K}\left(\left(N+1\right)^3+2K+n_2\left(\left(N+1\right)^2+5K\right)+n_2^2\right)\Big)$ where $n_2=\mathcal{O}\left(\left(N+1\right)^2\right)$. Thus, the approximate complexity of DBLDI-based AO is $o_{\mathbf{W}_T}+o_{\mathbf{\Phi}-\mathrm{DBLDI}}$.
- *BTI-based AO algorithm:* The approximate complexity of BTI-based AO is $o_{\mathbf{W}_T}+o_{\mathbf{\Phi}-\mathrm{BTI}}$, where the complexity of $o_{\mathbf{W}_T}$ is the same as DBLDI-based AO, and that of $o_{\mathbf{\Phi}-\mathrm{BTI}}$ is $\mathcal{O}\Big(n_2\sqrt{N+1+6K}\left(\left(N+1\right)^3+2K+n_2\left(\left(N+1\right)^2+4K\right)+n_2^2\right)\Big)$. It is found that the complexity of BTI-based AO is lower than that of DBLDI-based AO per iteration due to the fact that problem $\mathcal{Q}_B^V$ has one less SOC than $\mathcal{Q}_D^V$.
- *Low complexity algorithm (LCA) without jammer's CSI:* The approximate complexity of LCA is $o_{\mathbf{W}_T}+o_{\mathbf{\Phi}-\mathrm{LC}}$, where $o_{\mathbf{\Phi}-\mathrm{LC}} = \mathcal{O}\left(n_2\sqrt{N+1}\left(\left(N+1\right)^3+n_2(N+1)^2+n_2^2\right)\right)$. Obviously, the LCA has lowest complexity as compared with the other two algorithms.

VI. Simulation Results

In this section, numerical results are provided to validate the performance of the proposed algorithms. According to [31] and [33], the jammer is always deployed close to the users and interrupts the communications by sending the jamming signal to the the nearest user such that the maximal damage effect can be achieved. Thus, as shown in Fig. 2, we consider a 2D coordinate system, where the location of BS and IRS is (0m, 0m) and (10m, 5m), respectively, the users are uniformly distributed in a circle centered at (100m, 0m) with radius of 5m and the jammer is located at (125m, -5m). In addition, the jammer's beamforming is set to $\mathbf{w}_J = \sqrt{P_J}\frac{\widehat{\mathbf{h}}_{J,knear}}{\left\|\widehat{\mathbf{h}}_{J,knear}\right\|_2}$ in general, where $knear$ denotes the nearest user to jammer [33]. By reffering to [27], [31], [33], the number of BS antennas and jammer's antennas are set to $M = 8$ and $L = 2$, respectively.

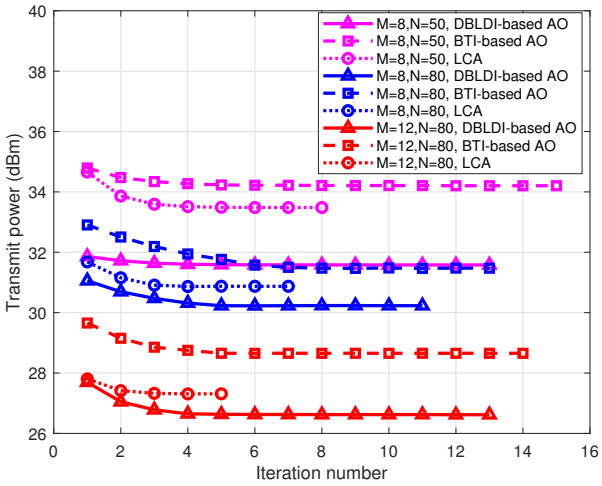

Fig. 3: Transmit power versus iteration number for different algorithms, when $P_J = 50$ dBm and $[\delta_{HJ}, \delta_{hJ}] = [0.2, 0.45]$.

The number of reflecting elements of the IRS is $N = N_xN_y$, where N_x is the number of IRS elements along with x-axis and N_y is that along y-axis. For brevity, we fix $N_x = 10$ and linearly increase N_y with N. We set the path loss exponent of BS-user link, jammer-user link, BS-IRS link, IRS-user link, and jammer-IRS link as $\iota_{BU} = \iota_{JU} = 4$ and $\iota_{BI} = \iota_{IU} = \iota_{JI} = 2$ [60]. Based on the 3GPP UMi model [60], the path loss reference L_0 is -10 dB with the reference distance $D_0 = 1$ m. In terms of the small scale fading, we set the Rician factors of all links involved are set to 1 [27]. For the jammer's statistical CSI error, the variance of $\mathrm{vec}(\Delta\mathbf{H}_{J,k})$ and $\Delta\mathbf{h}_{J,k}$ are defined as $\varepsilon_{H_{J,k}}^2 = \delta_{H_J}^2\left\|\widehat{\mathbf{H}}_{J,k}\right\|_F^2$ and $\varepsilon_{h_{J,k}}^2 = \delta_{h_J}^2\left\|\widehat{\mathbf{h}}_{J,k}\right\|_2^2$, respectively. $\delta_{hJ} \in [0,1)$ and $\delta_{HJ} \in [0,1)$ denote the CSI uncertainties. Other system settings as follows: the maximun outage probabilities are set to $\rho_1 = \cdots = \rho_K = 0.05$, the SINR targets are $\gamma_1 = \cdots = \gamma_K = 10$ dB, the noise power is set to $\sigma_1 = \cdots = \sigma_K = 10^{-9}$ W [33], the maximum iteration number $T_{max} = 50$, the convergence tolerance $\epsilon = 10^{-4}$, and the jamming power P_J ranges from 20 dBm to 80 dBm. The following simulation results are averaged over 300 random channel realizations.

First, the convergence of proposed three algorithms is illustrated in Fig. 3. Here, the jamming power is set as $P_J = 50$ dBm and the channel uncertainty coefficient is chosen as $[\delta_{HJ}, \delta_{hJ}] = [0.2, 0.45]$. It is apparent that for different M and N, all the proposed algorithms converge within 15 iterations. It is also observed that the LCA outperforms the other two algorithms significantly in terms of convergence, which suggests that LCA has the lowest implementation complexity. In addition, the rate of convergence increases with the number of IRS elements N, while that decreases with the number of transmit antennas M.

For the computational complexity, we evaluate that of proposed algorithms in terms of CPU time [61]. Fig. 4 compares the average CPU time of different algorithms versus the number of IRS elements N for different M. We obtain the

results by using a computer with a 2.90GHz R7-4800H CPU and 16GB RAM. Here, we still set $P_J = 50$ dBm and $[\delta_{HJ}, \delta_{hJ}] = [0.2, 0.45]$. The LCA requires much less CPU time than that required by the other two algorithms. This is due to the fact that the problem $\mathcal{Q}_P^V$ in LCA has less SOCs and its convergence speed is faster. Moreover, owing to the fact that the BTI-based AO requires more iterations to converge than the DBLDI-based AO, the CPU time of DBLDI-based AO is less than that of BTI-based AO for all considered M and N. Finally, we can observe the CPU time increases with the number of transmit antennas M and IRS elements N.

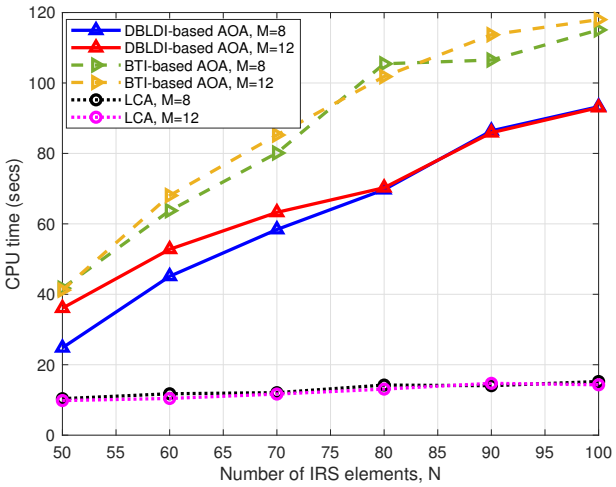

Fig. 4: Average CPU time versus the number of IRS elements N, when $P_J = 50$ dBm and $[\delta_{HJ}, \delta_{hJ}] = [0.2, 0.45]$.

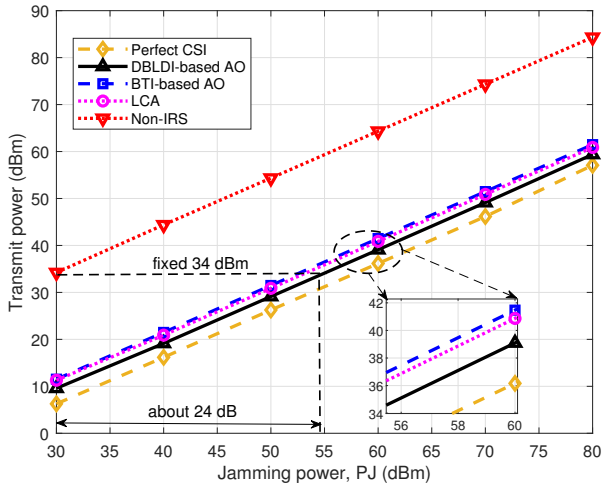

Fig. 5: Transmit power versus the jamming power P_J, when $M = 8$ and $[\delta_{HJ}, \delta_{hJ}] = [0.2, 0.45]$.

Fig. 5 shows the minimum transmit power for anti-jamming versus the jamming power P_J. For $M = 8$ and $[\delta_{HJ}, \delta_{hJ}] = [0.2, 0.45]$. It is found that the proposed three algorithms can significantly decrease the minimum transmit power as compared with non-IRS scheme. In addition, for fixed system energy supply, the jamming margin can be improved by jointly designing the active and passive beamforming. Pariticularly,

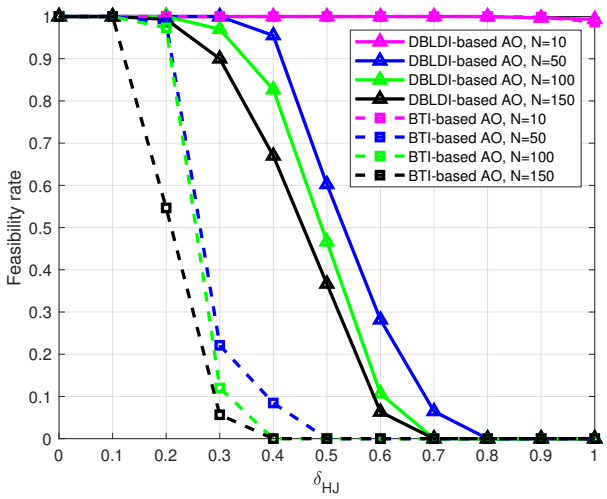

Fig. 6: Feasibility rate versus channel uncertainty level δ_{HJ}, when $P_J = 50$ dBm, $M = 8$ and $\delta_{hJ} = 0$.

when the transmit power is fixed as 34dBm, the non-IRS scheme can only combats the jamming power about 30 dBm, while the proposed algorithms can resist that about 55 dBm, and thus the jamming margin is significantly improved. Hence, compared to the scheme without IRS, proposed algorithms have better anti-jamming performamce and lower power consumption. With the presence of statistical channel, both the DBLDI-based AO and the BTI-based AO require more transmit power than that required by the scheme with perfect CSI, and the DBLDI-based AO requires less than the BTI-based AO. This phenomenon implies that the DBLDI-based AO is more suitable to the case with jammer's statistical CSI in the IRS-assisted anti-jamming system. Apparently, the performance of LCA is worse than the perfect CSI scheme, but better than the BTI-based AO. This is because the high level of channel uncertainties leads to the worst performance to the BTI-based AO, which also suggests that the LCA achieves a satisfactory complexity-preformance trade-off.

In what follows, we investigate the impact of channel uncertainty on the system performance. Fig. 6 and 7 show the feasibility rate versus the level of channel uncertainty δ_{HJ} and δ_{hJ}, respectively. In Fig. 6, we only consider the reflected channel uncetainty, i.e., $\delta_{hJ} = 0$. On the contrary, Fig. 7 only assumes direct channel uncetainty, i.e., $\delta_{HJ} = 0$. The feasibility rate is defined as the ratio of the number of feasible channel realization to the total number of channel realization, where feasible channel means there exists a feasible solution to problem $\mathcal{Q}_D^V$ and $\mathcal{Q}_B^V$ under this realization [34]. From Fig. 6 and 7, we can observe that the feasibility rate decreases with the increase of both channel uncertainty level and the number of IRS elements N, and δ_{HJ} has a greater impact on feasibility rate than δ_{hJ}. This is owing to the fact that δ_{HJ} is associated with N, which will lead to the increase of total channel estimation errors. Thus, both the RIS units number N and channel uncertainty level need to be carefully limited for the satisfactory feasibility perfromance. In addition, the DBLDI-based AO outperforms the BTI-based AO in terms of

feasibility rate for the fixed channel uncertainty level.

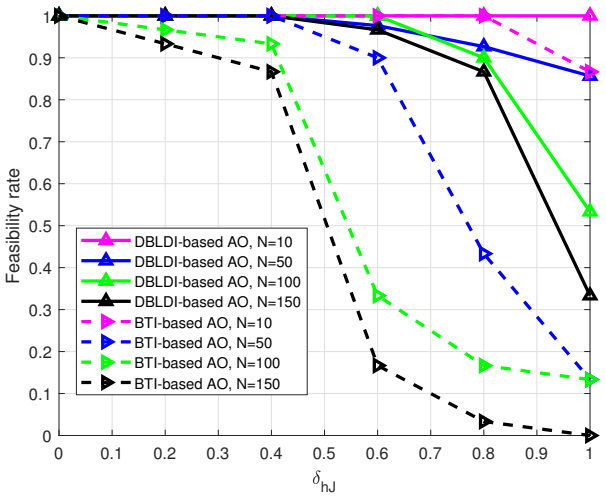

Fig. 7: Feasibility rate versus channel uncertainty level δ_{hJ}, when $P_J = 50$ dBm, $M = 8$ and $\delta_{HJ} = 0$.

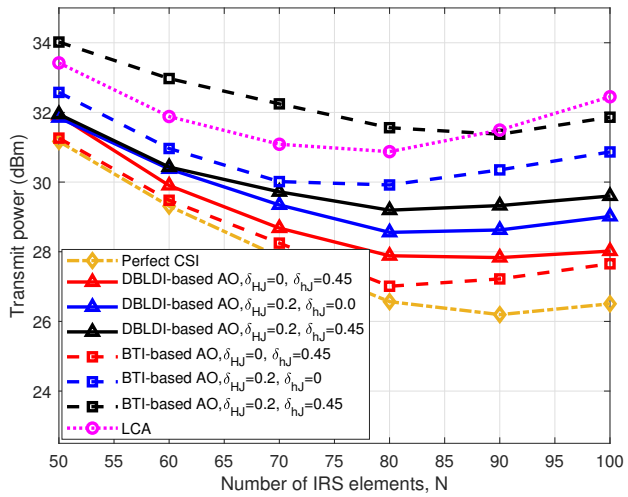

Fig. 8: Transmit power versus number of IRS elements N, when $P_J = 50$ dBm and $M = 8$.

Fig. 8 depicts that the transmit power of proposed algorithms versus the number of IRS elements for different channel uncertainty levels, where the values of uncertainty are employed according to feasibility analysis in Fig. 6 and 7. It obvious to find that the transmit power decreases with the number of IRS elements N when $N \leq 80$, along with a slightly reversed trend for $N > 80$. This is due to the fact that increasing IRS elements N can not only decreases the transmit power, but also increases both channel estimation error and jamming power that more transmit power is required. For the DBLDI-based AO and BTI-based AO, the power consumption under channel uncertainty is higher than that of perfect CSI, and the performance loss intensifies with the increase of channel uncertainty level. The reason can be explained by the fact that the BS needs to consume additional power to compensate for the outage loss caused by channel uncertainty. Moreover, the BTI-based AO is superior of the DBLDI-based

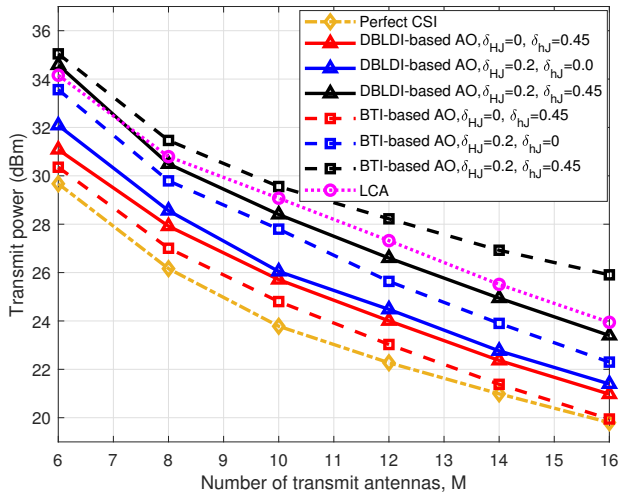

Fig. 9: Transmit power versus number of transmit antennas M, when $P_J = 50$ dBm and $N = 80$.

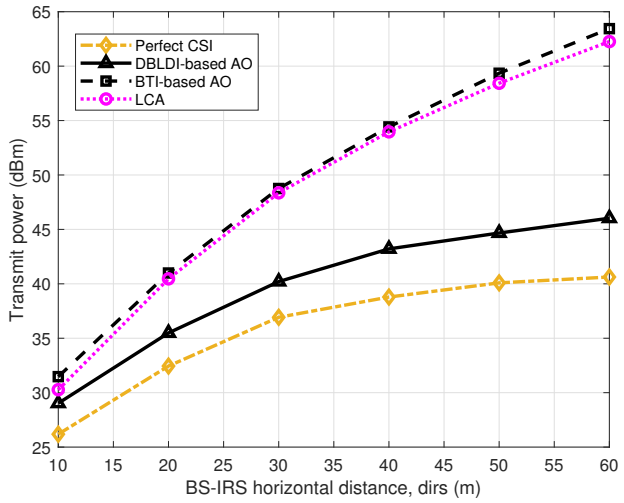

Fig. 10: Transmit power versus BS-IRS horizontal distance d_{irs}, when $P_J = 50$ dBm, $N = 80$, $M = 8$, and $[\delta_{HJ}, \delta_{hJ}] = [0.2, 0.45]$.

AO for a low channel uncertainty. On the other hand, δ_{HJ} has a greater impact on the transmit power than δ_{hJ}, which is owing to the fact that δ_{HJ} is associated with the IRS and the units at IRS will inrecase the channel uncertainty.

The transmit power versus the number of transmit antennas is shown in Fig. 9. It is observed that the transmit power consumption decreases with the number of transmit antennas even when the channel uncertainty values are large. This is because the large M increases the degrees of freedom which can be utilized to design the transmit beamforming at the BS.

Additionally, we examine the optimal deployment of IRS. Fig. 10 shows the transmit power versus the BS-IRS horizontal distance. The transmit power increases significantly with the BS-IRS horizontal distance d_{irs}. This is because when the IRS moves closer to the users, increasing d_{irs} can not only improve the desired signal power, but also increase the

reflected jamming power that more transmit power is required to combat it. Consequently, we can deploy the IRS near the BS, which facilitates our usage of IRS in practical.

VII. Conclusions

In this paper, we have studied robust beamforming optimization in a multiuser IRS-assisted anti-jamming communications system, for the cases with imperfect jammer's CSI and without jammer's CSI. Additionally, the fact that the jammer's transmit beamforming can not be known at BS were further considered in this paper. Specifically, with no knowledge of jammer's transmit beamforming, we aim to minimize the transmit power subjects to outage rate constraints under the jammer's statistical CSI and the SINR constraints with no jammer's CSI, respectively. The unknown jammer's beamformin issue was tackled by utilizing the use-and-then-forget (Uatf) method and Cauchy-Schwarz inequality, and then the jammer's statistical CSI uncertainties were addressed by using Decomposition-based large deviation inequality and Bernstein-type inequality. The case without jammer's CSI was dealt by the weighted channel gain method. Finally, applying the penalty non-smooth optimization method, the optimal rank-one solutions to the reformulated problems can be obtained in an iterative manner. Numerical results showed that proposed three algorithms have higher jamming margin and lower power consumption as compared with the scheme without IRS. In addition, the DBLDI-based AO outperformed the BTI-based AO in terms of transmit power, convergence, feasibility and complexity, and the LCA achieved a satisfactory complexity-preformance trade-off for the practical implementation. This paper also provided some useful insights for the optimal selection of the number of IRS elements and IRS deployment.

Appendix A
Proof of Proposition 1

First, problem $\mathcal{Q}_3^W$ is presented for the following derivation, which is given by

$$\mathcal{Q}_3^W: \min_{\mathbf{\Gamma}_T} \sum_{k=1}^{K} \left((\mu_k+1)\,\mathrm{Tr}\left\{\mathbf{\Gamma}_{T,k}\right\} - \mu_k \lambda_{\max}\left\{\mathbf{\Gamma}_{T,k}\right\}\right) \quad \text{(A.1)}$$
$$s.t.\ (12b), (12c).$$

Then, given a feasible solution $\left\{\mathbf{\Gamma}_{T,k}^{(n-1)}\right\}$ to problem $\mathcal{Q}_3^W$, we can obtain the optimal solution $\left\{\mathbf{\Gamma}_{T,k}^{(n)}\right\}$ by solving the following problem,

$$\begin{aligned}\hat{\mathcal{Q}}^W: \quad & \sum_{k=1}^{K}\Big\{(\mu_k+1)\,\mathrm{Tr}\left\{\mathbf{\Gamma}_{T,k}\right\} - \mu_k\lambda_{\max}\left\{\mathbf{\Gamma}_{T,k}^{(n)}\right\} \\ & -\mu_k\left\langle \mathbf{w}_{T,k,\max}^{(n-1)}\mathbf{w}_{T,k,\max}^{(n-1),H}, \mathbf{\Gamma}_{T,k}-\mathbf{\Gamma}_{T,k}^{(n)}\right\rangle \quad \text{(A.2)} \\ & s.t.\ (12b), (12c).\end{aligned}$$

Next, we use (16) to derive the relationship between nth and $(n-1)$th iteration, which is written as

$$\begin{aligned}& \sum_{k=1}^{K}\Big((\mu_k+1)\,\mathrm{Tr}\left\{\mathbf{\Gamma}_{T,k}^{(n)}\right\} - \mu_k\lambda_{\max}\left\{\mathbf{\Gamma}_{T,k}^{(n)}\right\}\Big) && \text{(A.3a)} \\ \le & \sum_{k=1}^{K}\Big\{(\mu_k+1)\,\mathrm{Tr}\left\{\mathbf{\Gamma}_{T,k}^{(n)}\right\} - \mu_k\lambda_{\max}\left\{\mathbf{\Gamma}_{T,k}^{(n-1)}\right\} \\ & \qquad -\mu_k\left\langle \mathbf{w}_{T,k,\max}^{(n-1)}\mathbf{w}_{T,k,\max}^{(n-1),H}, \mathbf{\Gamma}_{T,k}^{(n)}-\mathbf{\Gamma}_{T,k}^{(n-1)}\right\rangle\Big\} && \text{(A.3b)} \\ \le & \sum_{k=1}^{K}\Big((\mu_k+1)\,\mathrm{Tr}\left\{\mathbf{\Gamma}_{T,k}^{(n-1)}\right\} - \mu_k\lambda_{\max}\left\{\mathbf{\Gamma}_{T,k}^{(n-1)}\right\}\Big). && \text{(A.3c)}\end{aligned}$$

Evidently, we can achieve a better solution $\left\{\mathbf{\Gamma}_{T,k}^{(n)}\right\}$ to problem $\mathcal{Q}_3^W$ by solving problem $\hat{\mathcal{Q}}^W$. Moreover, if we remove the constant part in the objective function, problem $\hat{\mathcal{Q}}^W$ is equivalent to $\mathcal{Q}^W$. Thus, the optimal solution to problem $\mathcal{Q}_3^W$ can be obtained via solving $\mathcal{Q}^W$.

Hence, the proof is completed.

Appendix B
Proof of (20)

For ease of exposition, ζ_1 (20) is rewritten as follows:

$$\begin{aligned}\zeta_1 =& \Delta\mathbf{h}_{J,k}^H\left(-\mathbf{\Gamma}_J\right)\Delta\mathbf{h}_{J,k} + \mathbf{v}^H\Delta\mathbf{H}_{J,k}\left(-\mathbf{\Gamma}_J\right)\Delta\mathbf{H}_{J,k}^H\mathbf{v} \\ & + 2\mathrm{Re}\left\{\mathbf{v}^H\Delta\mathbf{H}_{J,k}\left(-\mathbf{\Gamma}_J\right)\Delta\mathbf{h}_{J,k}\right\} \\ =& -\varepsilon_{hJ,k}^2\mathbf{e}_{hJ,k}^H\mathbf{\Gamma}_J\mathbf{e}_{hJ,k} - \varepsilon_{HJ,k}^2\mathbf{e}_{HJ,k}\left(\mathbf{V}^T\otimes\mathbf{\Gamma}_J\right)\mathbf{e}_{HJ,k}^* \\ & - 2\mathrm{Re}\left\{\varepsilon_{HJ,k}\varepsilon_{hJ,k}\mathbf{e}_{HJ,k}^*\left(\mathbf{v}^*\otimes\mathbf{\Gamma}_J\right)\mathbf{e}_{hJ,k}^H\right\}, \qquad \text{(A.4)}\end{aligned}$$

It is not difficult to convert the first term inside ζ_1 to the second equality by defining $\Delta\mathbf{h}_{J,k} = \varepsilon_{hJ,k}\mathbf{e}_{hJ,k}$.

Then, the derivations of remaining terms inside ζ_1 follows $\mathcal{D}^{\zeta_1}$ at the top of this page, where the step (c) in (A.5) is derived from $\mathrm{vec}\left(\mathbf{A}^H\right)\mathrm{vec}\left(\mathbf{B}\right) = \mathrm{Tr}\left\{\mathbf{A}^H\mathbf{B}\right\}$, and the step (d) in (A.5) is obtained by $\mathrm{Tr}\left\{\mathbf{ABCD}\right\} = \mathrm{vec}\left(\mathbf{D}\right)\left(\mathbf{C}^T\otimes\mathbf{A}\right)\mathrm{vec}\left(\mathbf{B}\right)$.

Hence, the proof is completed.

Appendix C
Proof of Rank-one Constraints (36)

As analyzed in Section III-B, the rank-one constraints (34f) can be equivalently transformed into

$$\mathrm{rank}\left(\widehat{\mathbf{V}}\right) = 1 \Leftrightarrow \mathrm{Tr}\left\{\widehat{\mathbf{V}}\right\} - \lambda_{\max}\left\{\widehat{\mathbf{V}}\right\} \le 0. \qquad \text{(A.6)}$$

We also adopt the subgradient of $\lambda_{\max}\left\{\widehat{\mathbf{V}}\right\}$ to deal with its non-smoothness, which is given by

$$\partial\lambda_{\max}\left\{\widehat{\mathbf{V}}\right\} = \widehat{\mathbf{v}}_{\max}\widehat{\mathbf{v}}_{\max}^H, \qquad \text{(A.7)}$$

where $\widehat{\mathbf{v}}_{\max}$ is the eigenvector related with the maximum eigenvalue of $\lambda_{\max}\left\{\widehat{\mathbf{V}}\right\}$. Thus, by defining the feasible solution $\widehat{\mathbf{v}}_{\max}^{(n-1)}$ obtained at $(n-1)$th iteration, the first-order approximation of $\lambda_{\max}\left\{\widehat{\mathbf{V}}\right\}$ can be expressed as

$$\lambda_{\max}\left\{\widehat{\mathbf{V}}\right\} - \lambda_{\max}\left\{\widehat{\mathbf{V}}^{(n-1)}\right\} \ge \left\langle \widehat{\mathbf{v}}_{\max}^{(n-1)}\widehat{\mathbf{v}}_{\max}^{(n-1),H}, \widehat{\mathbf{V}} - \widehat{\mathbf{V}}^{(n-1)}\right\rangle. \qquad \text{(A.8)}$$

$$
\begin{aligned}
\mathcal{D}^{\zeta_1}: \ & \mathbf{v}^H \Delta\mathbf{H}_{J,k} \left(-\mathbf{\Gamma}_J\right) \Delta\mathbf{H}_{J,k}^H \mathbf{v} + 2\mathrm{Re}\left\{\mathbf{v}^H \Delta\mathbf{H}_{J,k} \left(-\mathbf{\Gamma}_J\right) \Delta\mathbf{h}_{J,k}\right\} \\
\overset{a}{=} \ & \mathrm{vec}^H\left(\Delta\mathbf{H}_{J,k}\right) \mathrm{vec}\left(\mathbf{V}\Delta\mathbf{H}_{J,k}\left(-\mathbf{\Gamma}_J\right)\right) + 2\mathrm{Re}\left\{\mathrm{vec}^H\left(\Delta\mathbf{h}_{J,k}\right) \mathrm{vec}\left(\mathbf{v}^H\Delta\mathbf{H}_{J,k}\left(-\mathbf{\Gamma}_J\right)\right)\right\} \\
\overset{b}{=} \ & \left\{\mathrm{vec}^H\left(\mathbf{V}\Delta\mathbf{H}_{J,k}\left(-\mathbf{\Gamma}_J\right)\right) \mathrm{vec}\left(\Delta\mathbf{H}_{J,k}\right)\right\}^H + 2\mathrm{Re}\left\{\left\{\mathrm{vec}^H\left(\mathbf{v}^H\Delta\mathbf{H}_{J,k}\left(-\mathbf{\Gamma}_J\right)\right) \mathrm{vec}\left(\Delta\mathbf{h}_{J,k}\right)\right\}^H\right\} \\
\overset{c}{=} \ & \left\{\mathrm{Tr}\left\{\left(-\mathbf{\Gamma}_J\right)\Delta\mathbf{H}_{J,k}^H\mathbf{V}^H\Delta\mathbf{H}_{J,k}\right\}\right\}^H + 2\mathrm{Re}\left\{\left\{\mathrm{Tr}\left\{\left(-\mathbf{\Gamma}_J\right)\Delta\mathbf{H}_{J,k}^H\mathbf{v}\Delta\mathbf{h}_{J,k}\right\}\right\}^H\right\} \\
\overset{d}{=} \ & \left\{\mathrm{vec}^T\left(\Delta\mathbf{H}_{J,k}\right)\left(\mathbf{V}^* \otimes \left(-\mathbf{\Gamma}_J\right)\right) \mathrm{vec}\left(\Delta\mathbf{H}_{J,k}^H\right)\right\}^H + 2\mathrm{Re}\left\{\left\{\Delta\mathbf{h}_{J,k}^T\left(\mathbf{v}^T \otimes \left(-\mathbf{\Gamma}_J\right)\right) \mathrm{vec}^H\left(\Delta\mathbf{H}_{J,k}\right)\right\}^H\right\} \\
\overset{e}{=} \ & -\varepsilon_{HJ,k}^2 \mathbf{e}_{HJ,k}\left(\mathbf{V}^T \otimes \mathbf{\Gamma}_J\right)\mathbf{e}_{HJ,k}^* - 2\mathrm{Re}\left\{\varepsilon_{HJ,k}\varepsilon_{hJ,k}\mathbf{e}_{HJ,k}^*\left(\mathbf{v}^* \otimes \mathbf{\Gamma}_J\right)\mathbf{e}_{hJ,k}^H\right\}
\end{aligned} \tag{A.5}
$$

As such, the term $\mathrm{Tr}\left\{\widehat{\mathbf{V}}\right\} - \lambda_{\max}\left\{\widehat{\mathbf{V}}\right\} \leq 0$ can be rewritten as

$$
\begin{aligned}
& \mathrm{Tr}\left\{\widehat{\mathbf{V}}\right\} - \lambda_{\max}\left\{\widehat{\mathbf{V}}\right\} \leq \tau \\
\Rightarrow & \mathrm{Tr}\left\{\widehat{\mathbf{V}}\right\} - \lambda_{\max}\left\{\widehat{\mathbf{V}}^{(n-1)}\right\} - \left\langle \widehat{\mathbf{v}}_{\max}^{(n-1)}\widehat{\mathbf{v}}_{\max}^{(n-1),H}, \widehat{\mathbf{V}} - \widehat{\mathbf{V}}^{(n-1)}\right\rangle \leq \tau
\end{aligned} \tag{A.9}
$$

where τ is a penalty parameter. Note that the function above can be further simplified as

$$
\mathrm{Tr}\left\{\widehat{\mathbf{V}}\right\} - \left\langle \widehat{\mathbf{v}}_{\max}^{(n-1)}\widehat{\mathbf{v}}_{\max}^{(n-1),H}, \widehat{\mathbf{V}}\right\rangle \leq \tau, \tag{A.10}
$$

which is due to the property that

$$
\lambda_{\max}\left\{\widehat{\mathbf{V}}^{(n-1)}\right\} = \widehat{\mathbf{v}}_{\max}^{(n-1),H}\widehat{\mathbf{V}}^{(n-1)}\widehat{\mathbf{v}}_{\max}^{(n-1)}. \tag{A.11}
$$

Hence, the proof is completed.

REFERENCES

[1] L. Chettri and R. Bera, "A comprehensive survey on internet of things (IoT) toward 5g wireless systems," *IEEE Internet Things J.*, vol. 7, no. 1, pp. 16–32, 2020.

[2] F. Guo, F. R. Yu, H. Zhang, X. Li, H. Ji, and V. C. Leung, "Enabling massive iot toward 6g: A comprehensive survey," *IEEE Internet Things J.*, pp. 1–1, 2021.

[3] Y. Zou, J. Zhu, X. Wang, and L. Hanzo, "A survey on wireless security: Technical challenges, recent advances, and future trends," *Proc. IEEE*, vol. 104, no. 9, pp. 1727–1765, 2016.

[4] M. K. Hanawal, M. J. Abdel-Rahman, and M. Krunz, "Joint adaptation of frequency hopping and transmission rate for anti-jamming wireless systems," *IEEE Trans. Mobile Comput.*, vol. 15, no. 9, pp. 2247–2259, 2016.

[5] A. Gouissem, K. Abualsaud, E. Yaacoub, T. Khattab, and M. Guizani, "Game theory for anti-jamming strategy in multi-channel slow fading iot networks," *IEEE Internet Things J.*, pp. 1–1, 2021.

[6] W. Xu, T. Wood, W. Trappe, and Y. Zhang, "Channel surfing and spatial retreats: Defenses against wireless denial of service," in *Proceedings of the 2004 ACM Workshop on Wireless Security, WiSe*, 2004.

[7] P. Gu, C. Hua, W. Xu, R. Khatoun, Y. Wu, and A. Serhrouchni, "Control channel anti-jamming in vehicular networks via cooperative relay beamforming," *IEEE Internet Things J.*, vol. 7, no. 6, pp. 5064–5077, 2020.

[8] Y. Gao, Y. Xiao, M. Wu, M. Xiao, and J. Shao, "Game theory-based anti-jamming strategies for frequency hopping wireless communications," *IEEE Trans. Wireless Commun.*, vol. 17, no. 8, pp. 5314–5326, 2018.

[9] J. Zheng, Y. Cai, and A. A. Xu, Y, "Distributed channel selection for interference mitigation in dynamic environment: A game-theoretic stochastic learning solution," *IEEE Trans. Veh. Technol.*, vol. 63, no. 9, pp. 4757–4762, 2014.

[10] Y. Wu, B. Wang, K. J. R. Liu, and T. C. Clancy, "Anti-jamming games in multi-channel cognitive radio networks," *IEEE J. Sel. Areas Commun.*, vol. 30, no. 1, pp. 4–15, 2011.

[11] X. Liu, Y. Xu, L. Jia, Q. Wu, and A. Anpalagan, "Anti-jamming communications using spectrum waterfall: A deep reinforcement learning approach," *IEEE Commun. Lett.*, pp. 1–1, 2017.

[12] F. Yao and L. Jia, "A collaborative multi-agent reinforcement learning anti-jamming algorithm in wireless networks," *IEEE Wireless Commun. Lett.*, vol. 8, no. 4, pp. 1024–1027, 2019.

[13] L. Jia, F. Yao, Y. Sun, Y. Niu, and Y. Zhu, "Bayesian stackelberg game for antijamming transmission with incomplete information," *IEEE Commun. Lett.*, vol. 20, no. 10, pp. 1991–1994, 2016.

[14] L. Jia, F. Yao, Y. Sun, Y. Xu, S. Feng, and A. Anpalagan, "A hierarchical learning solution for anti-jamming stackelberg game with discrete power strategies," *IEEE Wireless Commun. Lett.*, vol. 6, no. 6, pp. 818–821, 2017.

[15] A. Garnaev, A. Petropulu, W. Trappe, and H. V. Poor, "A power control game with uncertainty on the type of the jammer," in *2019 IEEE Global Conference on Signal and Information Processing (GlobalSIP)*, 2019.

[16] Z. Dou, G. Si, Y. Lin, and M. Wang, "An adaptive resource allocation model with anti-jamming in iot network," *IEEE Access*, vol. 7, pp. 93 250–93 258, 2019.

[17] Q. Yan, H. Zeng, T. Jiang, M. Li, W. Lou, and Y. T. Hou, "MIMO-based jamming resilient communication in wireless networks," in *IEEE INFOCOM*, 2014, pp. 2697–2706.

[18] Q. Liu, M. Li, X. Kong, and N. Zhao, "Disrupting MIMO communications with optimal jamming signal design," *IEEE Trans. Wireless Commun.*, vol. 14, no. 10, pp. 5313–5325, 2015.

[19] G. Yu, X. Chen, C. Zhong, D. W. Kwan Ng, and Z. Zhang, "Design, analysis, and optimization of a large intelligent reflecting surface-aided b5g cellular internet of things," *IEEE Internet Things J.*, vol. 7, no. 9, pp. 8902–8916, 2020.

[20] S. Kisseleff, W. A. Martins, H. Al-Hraishawi, S. Chatzinotas, and B. Ottersten, "Reconfigurable intelligent surfaces for smart cities: Research challenges and opportunities," *IEEE Open J. of the Commun. Society*, vol. 1, pp. 1781–1797, 2020.

[21] X. Lei, M. Wu, F. Zhou, X. Tang, R. Q. Hu, and P. Fan,"Reconfigurable intelligent surface-based symbiotic radio for 6G: Design, challenges, and opportunities," *IEEE Wireless Commun.*, vol. 28, no. 5, pp. 210–216, 2021.

[22] C. Pan, H. Ren, K. Wang, M. Elkashlan, A. Nallanathan, J. Wang, and L. Hanzo, "Intelligent reflecting surface aided MIMO broadcasting for simultaneous wireless information and power transfer," *IEEE J. Sel. Areas Commun.*, vol. 38, no. 8, pp. 1719–1734, 2020.

[23] Q. Wu and R. Zhang, "Intelligent reflecting surface enhanced wireless network via joint active and passive beamforming," *IEEE Trans. Wireless Commun.*, vol. 18, no. 11, pp. 5394–5409, 2019.

[24] ——, "Towards smart and reconfigurable environment: Intelligent reflecting surface aided wireless network," *IEEE Commun. Mag.*, vol. 58, no. 1, pp. 106–112, 2020.

[25] C. Huang, A. Zappone, G. C. Alexandropoulos, M. Debbah, and C. Yuen, "Reconfigurable intelligent surfaces for energy efficiency in wireless communication," *IEEE Trans. Wireless Commun.*, vol. 18, no. 99, pp. 4157–4170, 2019.

[26] Z. Chu, W. Hao, P. Xiao, and J. Shi, "Intelligent reflecting surface aided multi-antenna secure transmission," *IEEE Wireless Commun. Lett.*, vol. PP, no. 99, pp. 1–1, 2019.

[27] M. Cui, G. Zhang, and R. Zhang, "Secure wireless communication via intelligent reflecting surface," *IEEE Wireless Commun. Lett.*, vol. 8, no. 5, pp. 1410–1414, 2019.

[28] H. Han, J. Zhao, D. Niyato, M. D. Renzo, and Q. Pham, "Intelligent

reflecting surface aided network: Power control for physical-layer broadcasting," in *ICC 2020,*, pp. 1–7.
[29] X. Guan, Q. Wu, and R. Zhang, "Intelligent reflecting surface assisted secrecy communication: Is artificial noise helpful or not?" *IEEE Wireless Commun. Lett.*, vol. 9, no. 6, pp. 778–782, 2020.
[30] W. Hao, G. Sun, M. Zeng, Z. Chu, Z. Zhu, O. A. Dobre, and P. Xiao, "Robust design for intelligent reflecting surface assisted MIMO-OFDMA terahertz IoT networks," *IEEE Internet of Things Journal*, pp. 1–1, 2021.
[31] H. Yang, Z. Xiong, J. Zhao, D. Niyato, Q. Wu, H. V. Poor, and M. Tornatore, "Intelligent reflecting surface assisted anti-jamming communications: A fast reinforcement learning approach," *IEEE Trans. Wireless Commun.*, 2020.
[32] Z. Shen, K. Xu, and X. Xia, "Beam-domain anti-jamming transmission for downlink massive MIMO systems: A stackelberg game perspective," *IEEE Trans. Inf. Forensics Security*, vol. 16, pp. 2727–2742, 2021.
[33] Y. Sun, K. An, J. Luo, Y. Zhu, G. Zheng, and S. Chatzinotas, "Intelligent reflecting surface enhanced secure transmission against both jamming and eavesdropping attacks," *IEEE Trans. Veh. Technol.*, vol. 70, no. 10, pp. 11 017–11 022, 2021.
[34] G. Zhou, C. Pan, H. Ren, K. Wang, and A. Nallanathan, "A framework of robust transmission design for IRS-aided MISO communications with imperfect cascaded channels," *IEEE Trans. Signal Process.*, vol. 68, pp. 5092–5106, 2020.
[35] L. Zhang, C. Pan, Y. Wang, H. Ren, K. Wang, and A. Nallanathan, "Robust beamforming design for intelligent reflecting surface aided cognitive radio systems with imperfect cascaded CSI," 2020, arXiv:2004.04595.
[36] X. Yu, D. Xu, Y. Sun, D. W. K. Ng, and R. Schober, "Robust and secure wireless communications via intelligent reflecting surfaces," *IEEE J. Sel. Areas Commun.*, vol. 38, no. 11, pp. 2637–2652, 2020.
[37] H. M. Wang, J. Bai, and L. Dong, "Intelligent reflecting surfaces assisted secure transmission without eavesdropper's CSI," *IEEE Signal Process. Lett.*, vol. PP, no. 99, pp. 1–1, 2020.
[38] H. Niu, Z. Chu, F. Zhou, Z. Zhu, L. Zhen, and K.-K. Wong, "Robust design for intelligent reflecting surface assisted secrecy swipt network," *IEEE Trans. Wireless Commun.*, pp. 1–1, 2021.
[39] S. Hu, Z. Wei, Y. Cai, C. Liu, D. W. K. Ng, and J. Yuan, "Robust and secure sum-rate maximization for multiuser MISO downlink systems with self-sustainable IRS," *IEEE Trans. Commun.*, vol. 69, no. 10, pp. 7032–7049, 2021.
[40] H. E. Gamal and E. Geraniotis, "Comparing FH/SSMA and DS/CDMA networks: capacity vs anti-jam margin tradeoff," in *IEEE Military Commun. Conference. Proc. MILCOM 98 (Cat. No.98CH36201)*, vol. 2, 1998, pp. 489–493 vol.2.
[41] G. Zhou, C. Pan, H. Ren, K. Wang, M. D. Renzo, and A. Nallanathan, "Robust beamforming design for intelligent reflecting surface aided MISO communication systems," *IEEE Wireless Commun. Lett.*, vol. 9, no. 10, pp. 1658–1662, 2020.
[42] X. Yu, V. Jamali, D. Xu, D. W. K. Ng, and R. Schober, "Smart and reconfigurable wireless communications: From IRS modeling to algorithm design," *arXiv: 2103.07046. [Online]. Available: https://arxiv.org/abs/2103.07046.*, 2021.
[43] S. Abeywickrama, R. Zhang, Q. Wu, and C. Yuen, "Intelligent reflecting surface: Practical phase shift model and beamforming optimization," *IEEE Trans. Commun.*, vol. 68, no. 9, pp. 5849–5863, 2020.
[44] C. Pan, H. Ren, K. Wang, M. Elkashlan, A. Nallanathan, J. Wang, and L. Hanzo, "Intelligent reflecting surface aided MIMO broadcasting for simultaneous wireless information and power transfer," *IEEE J. Sel. Areas Commun.*, vol. 38, no. 8, pp. 1719–1734, 2020.
[45] C. Cai, H. Yang, X. Yuan, and Y. C. Liang, "Two-timescale optimization for intelligent reflecting surface aided D2D underlay communication," 2020, arXiv:2006.01604.
[46] Z. Wang, L. Liu, and S. Cui, "Channel estimation for intelligent reflecting surface assisted multiuser communications: Framework, algorithms, and analysis," *IEEE Trans. Wireless Commun.*, vol. 19, no. 10, pp. 6607–6620, 2020.
[47] M.-M. Zhao, A. Liu, Y. Wan, and R. Zhang, "Two-timescale beamforming optimization for intelligent reflecting surface aided multiuser communication with QoS constraints," *IEEE Trans. Wireless Commun.*, vol. 20, no. 9, pp. 6179–6194, 2021.
[48] R. Schmidt, "Multiple emitter location and signal parameter estimation," *IEEE Trans. Antennas and Propag.*, vol. 34, no. 3, pp. 276–280, 1986.
[49] K. Y. Wang, M. C. So, T. H. Chang, W. K. Ma, and C. Y. Chi, "Outage constrained robust transmit optimization for multiuser MISO downlinks: Tractable approximations by conic optimization," *IEEE Trans. Signal Process.*, vol. 62, no. 21, pp. 5690–5705, 2014.
[50] A. H. Phan, "Nonsmooth optimization for efficient beamforming in cognitive radio multicast transmission," *IEEE Trans. Signal Process.*, vol. 60, no. 6, pp. 2941–2951, 2012.
[51] I. Bechar, "A bernstein-type inequality for stochastic processes of quadratic forms of gaussian variables," *Math.*, 2009.
[52] M. Bengtsson, "Optimal and suboptimal transmit beamforming," *Handbook of Antennas in Wireless Commun.*, 01 2001.
[53] A. Wiesel, Y. C. Eldar, and S. Shamai, "Linear precoding via conic optimization for fixed MIMO receivers," *IEEE Trans. Signal Process.*, vol. 54, no. 1, pp. 161–176, 2005.
[54] M. Grant and B. SP, "CVX: MATLAB software for disciplined convex programming," 2014.
[55] R. Nie, L. Chen, N. Zhao, Y. Chen, W. Wang, and X. Wang, "Impact and calibration of nonlinear reciprocity mismatch in massive MIMO systems," *IEEE Trans. Wireless Commun.*, vol. 20, no. 10, pp.6418–6435, 2021.
[56] R. Nie, L. Chen, N. Zhao, Y. Chen, F. R. Yu, and G. Wei, "Relaying systems with reciprocity mismatch: Impact analysis and calibration," *IEEE Trans. Commun.*, vol. 68, no. 7, pp. 4035–4049, 2020.
[57] L. Xiao, T. Chen, J. Liu, and H. Dai, "Anti-jamming transmission stackelberg game with observation errors," *IEEE Commun. Lett.*, vol. 19, no. 6, pp. 949–952, 2015.
[58] L. Xiao, J. Liu, Q. Li, N. B. Mandayam, and H. V. Poor, "User-centric view of jamming games in cognitive radio networks," *IEEE Trans. Inf. Forensics Security*, vol. 10, no. 12, pp. 2578–2590, 2015.
[59] Z. Lin, M. Lin, J. Ouyang, W.-P. Zhu, A. D. Panagopoulos, and M.-S. Alouini, "Robust secure beamforming for multibeam satellite communication systems," *IEEE Trans. Veh. Technol.*, vol. 68, no. 6, pp. 6202–6206, 2019.
[60] 3GPP, "Technical specification group radio access network; study on 3D channel model for LTE," 2017.
[61] J. Yuan, Y. C. Liang, J. Joung, G. Feng, and E. G. Larsson, "Intelligent reflecting surface-assisted cognitive radio system," *IEEE Trans. Commun.*, pp. 1–1, 2020.